Thiol-norbornene gelatin hydrogels: influence of thiolated crosslinker on network properties and high definition 3D printing

Biofabrication

OPEN ACCESS

RECEIVED
6 June 2020

REVISED
16 October 2020

ACCEPTED FOR PUBLICATION
11 November 2020

PUBLISHED
31 December 2020

PAPER

Thiol-norbornene gelatin hydrogels: influence of thiolated crosslinker on network properties and high definition 3D printing

Jasper Van Hoorick[1,2], Agnes Dobos[1,3,4], Marica Markovic[3,4], Tom Gheysens[1], Lana Van Damme[1], Peter Gruber[1,3], Liesbeth Tytgat[1,2], Jürgen Van Erps[2], Hugo Thienpont[1,2], Peter Dubruel[1], Aleksandr Ovsianikov[3,4] and Sandra Van Vlierberghe[1,2]

[1] Polymer Chemistry and Biomaterials Group, Centre of Macromolecular Chemistry, Department of Organic and Macromolecular Chemistry, Ghent University, Ghent, Belgium

[2] Brussels Photonics, Department of Applied Physics and Photonics, Flanders Make and Vrije Universiteit Brussel, Pleinlaan 2, Brussels, Belgium

[3] 3D Printing and Biofabrication Research Group, Institute of Materials Science and Technology, Technische Universität Wien (TU Wien), Vienna, Austria

[4] Austrian Cluster for Tissue Regeneration www.tissue-regeneration.at.

E-mail: Sandra.vanvlierberghe@ugent.be

Keywords: gelatin, thiol-ene chemistry, crosslinker, multiphoton lithography, biofabrication

Supplementary material for this article is available online

Abstract

Photocrosslinkable gelatin hydrogels are excellent bioinks or biomaterial ink components to serve biofabrication applications. Especially the widely investigated gelatin-methacroyl (gel-MA) hydrogels hold an impressive track record. However, over the past decade, increasing attention is being paid to thiol-ene photo-click chemistry to obtain hydrogel networks benefitting from a faster reactivity (i.e. seconds vs minutes) along with superior biocompatibility and processability. In order to exploit this photo-click chemistry, often an ene-functionality (e.g. norbornene) is introduced onto gelatin followed by crosslinking in the presence of a multifunctional thiol (e.g. dithiothreitol). To date, very limited research has been performed on the influence of the applied thiolated crosslinker on the final hydrogel properties. Therefore, the present work assesses the influence of different thiolated crosslinkers on the crosslinking kinetics, mechanical properties and biological performance of the hydrogels upon encapsulation of primary adipose tissue-derived stem cells which indicated a cell viability exceeding 70%. Furthermore, the different formulations were processed using two-photon polymerization which indicated, in addition to differences in processing window and swelling ratio, a previously unreported phenomenon. At high intensities (i.e. $\geqslant$150 mW), the laser results in cleavage of the gelatin backbone even in the absence of distinct photo-cleavable functionalities. This can have potential to introduce channels or softer regions in gels to result in zones characterized by different degradation speeds or the formation of blood vessels. Consequently, the present study can be used to provide guidance towards tailoring the thiol-ene system towards the desired applications.

1. Introduction

Over the past two decades, gelatin and more specifically photo-crosslinkable derivatives have become very popular materials in the field of biofabrication and tissue engineering (TE). This is mainly due to its structural similarity to the natural extra-cellular matrix of tissues. This is because gelatin is derived from collagen, thereby resulting in a biodegradable hydrogel containing cell interactive tripeptide arginine-glycine-aspartic acid (RGD) motifs [1–5]. Furthermore, it exhibits an attractive cost combined with a large track record in the field of pharmacy and medicine [1, 6–9]. Additionally, there are numerous available protocols for straightforward processing [1]. Especially, the traditional gelatin-methacryloyl (gel-MOD (i.e. modified gelatin) also known as gel-MA (i.e. gelatin-methacryloyl)) derivatives have been used numerously due to the well-described chemical modification and ease-of-use [1, 10–13].

These derivatives can be crosslinked using a free radical chain-growth polymerization of the introduced methacryloyl functionalities in between the gelatin chains [12]. Although widely reported, these methacryloyl derivatives exhibit some drawbacks including the formation of non-biodegradable kinetic chains, the susceptibility to oxygen inhibition during polymerization and associated slower crosslinking reaction, and poor control over this crosslinking reaction [14]. Therefore, researchers have been looking into alternative crosslinking approaches to stabilise gelatin hydrogels at physiological conditions while ensuring straightforward processability. One of the most popular alternatives to date is thiol-ene chemistry, where an 'ene' functionality is reacted with a thiolated crosslinker. This process can be induced either by light or mild pH changes (i.e. thiol-Michael addition which takes place at slightly alkaline conditions being within physiological range [15]) and occurs under mild reaction conditions making it a suitable candidate for cell-encapsulation [1]. Furthermore, since two complementary functional groups are reacted with each other, the crosslinking occurs according to a step-growth based polymerization approach, leading to a network without the formation of kinetic chains [14, 16, 17]. When using the light induced approach, this generally occurs significantly faster (i.e. within seconds [1, 16]) in comparison to the conventional chain-growth approaches (i.e. several minutes [1, 16]). To apply thiol-ene chemistry to crosslink gelatin, the predominant approach is to introduce 'ene' functionalities to gelatin which can be crosslinked using a thiolated crosslinker [13, 14, 16, 18, 19]. One of the most popular 'ene'-functionalities is norbornene as it is not prone to competitive homopolymerization or pH induced thiol-Michael addition. Therefore, norbornene based thiol-ene systems result in a high degree of control on the number of reacted functionalities by varying the thiol-ene ratio [1, 16, 18, 20]. Furthermore, thiol-norbornene photo-crosslinking reactions are extremely fast due to ring-strain relief upon thyil addition and a very fast subsequent thiol hydrogen abstraction rate [14, 18, 21]. As a result, they can be processed at low intensities combined with fast processing thereby becoming highly attractive towards light-based additive manufacturing (AM) and especially (high resolution) light- or laser-based techniques including stereolithography (SLA), digital light projection (DLP) and two-photon polymerization (2PP) where the processing throughput is highly dependent on the maximally attainable scanning speed of the laser or minimal irradiation time, which is often limited by slow polymerization kinetics [1, 14, 16, 17, 19, 22]. Consequently, faster polymerizations can result in higher scanning/writing speeds (i.e. already up to 1000 mm s^{-1} for gelatin-norbornene (gel-NB)/dithiothreitol (DTT) systems) [16]. An additional benefit of this fast, more controlled reaction is the fact that the materials can be processed with excellent shape fidelity and high cell viability [17, 19, 22].

However, besides the fact that a lot of research has been performed on thiol-ene photo-click gelatin hydrogels, limited attention has been paid to an additional benefit of thiol-ene crosslinking chemistry. The crosslinking occurs via the reaction of complementary functionalities. Therefore the network properties and material processability can be influenced via variation of the thiol/ene ratio or the use of different thiolated crosslinkers [1]. In this respect, the most popular crosslinker to date is DTT, however other crosslinkers have also been reported including polyethylene glycol (PEG)- and gelatin based crosslinkers [14, 16, 18, 19, 23, 24]. Although different crosslinkers have already been reported, limited research has been performed on a direct comparison between the different thiolated crosslinkers on the processability and properties of the formulation.

Therefore, in the present work, gel-NB was developed with a high degree of substitution (DS) (i.e. 90%) to investigate the influence of six different thiolated crosslinkers on the hydrogel properties in terms of physico-chemical characteristics, biological performance upon encapsulating adipose tissue-derived stem cells (ASCs) and on the laser-based (2PP) processing potential. The applied crosslinkers are DTT as it is one of the most reported crosslinkers. Four thiolated PEGS (i.e. tetraethylene glycol dithiol, PEG dithiol with a molar mass of 3400 and PEG tetrathiol with a molar mass of 10 000 or 20 000) and a thiolated gelatin. The different PEGs were selected to assess the influence of molar mass and number of crosslinks on the performance. The thiolated gelatin (i.e. gel-SH with a DS of 72% (i.e. 0.28 mmol thiols/g gelatin)) was selected due to its structural similarities with gel-NB. In this respect, it is anticipated that no issues related to phase separation of both components will occur in contrast to what was previously reported when using different polymer backbones [1, 4]. All performed assays were benchmarked against gel-MOD with a comparable DS (i.e. 95%) as this is a commonly applied material in the field of biofabrication and TE [1, 12].

2. Materials and methods

2.1. Materials

Gelatin type B (from bovine hides) was kindly supplied by Rousselot (Ghent, Belgium); 3-(trimethoxysilyl)propyl methacrylate (98%); 5-norbornene-2-carboxylic acid (predominantly endo) (98%); D,L-DTT (⩾99%); DL-N-Acetylhomocysteine thiolactone (98%) and deuterium oxide (D_2O); dimethylsulfoxide (DMSO) (⩾99%); ethylenediaminetetraacetic acid (EDTA) tetrasodium tetrahydrate salt; KH_2PO_4 (⩾99%); LiBr (⩾99%); methacrylic anhydride (94%); Na_2HPO_4 (⩾99%); Na_2CO_3 (⩾99.5%); $NaHCO_3$ (⩾99.7%);

NaOH; poly(ethylene glycol) dithiol (3400 g mol^{-1}) (PEG2SH 3400) and tetra(ethylene glycol) dithiol (TEG2SH) (97%), DL-DTT (⩾98%) were purchased at Sigma-Aldrich (Diegem, Belgium). N-(3-dimethylaminopropyl)- N′-ethylcarbodiimide hydrochloride (EDC) (>98%) was obtained at TCI (Zwijndrecht, Belgium). N-hydroxysuccinimide (98%) (NHS) was purchased at Acros (Geel, Belgium). Irgacure 2959® (1-[4-(2-hydroxyethoxy)-phenyl]-2-hydroxy-2-methyl-1-propane-1-one) was purchased at BASF (Antwerp, Belgium). Fluorescein isothiocyanate (FITC)-dextran (2000 g mol^{-1}) was obtained from TdB Consultancy AB (Uppsala, Sweden). (2,4,6-trimethylbenzoyl)-phenylphosphinic acid ethyl ester (i.e. Speedcure TPO-L) was obtained from Lambson (West Yorkshire, UK).The 4-arm-PEG-SH-20k (PEG4SH 20k) and 4-arm-PEG-SH-10k (PEG4SH 10k) were obtained from Laysan Bio Inc. (Alabama, USA). The dialysis membranes Spectra/Por® (Cutoff 12.000–14.000 g mol^{-1}) were obtained from Polylab (Antwerp, Belgium). All chemicals were used as received unless stated otherwise.

2.2. Methods

2.2.1. Modification of the primary amines in gelatin

In the present work, gelatin was modified as indicated in figure 1, according to previously reported procedures [11, 16, 23].

2.2.1.1. Development of gel-MOD

Briefly, 100 g gelatin type B (38.5 mmol reactive amines) was dissolved in 1 l of phosphate buffer (pH 7.8) at 40 °C under continuous mechanical stirring. Next, 2.5 equivalents (equiv.) (i.e. 14.34 ml, 96.25 mmol) methacrylic anhydride were added and the mixture was allowed to react for 1 h to obtain gel-MOD with a high DS. After 1 h, the reaction mixture was diluted with 1 l double distilled water (DDW) (ρ = 18.2 MΩ cm) followed by dialysis against distilled water (molar mass cut-off 12 000–14 000 g mol^{-1}) during 24 h at 40 °C, with the water being changed five times. The pH of the solution was adjusted to ~7.4 using a 5 M NaOH solution. Finally, the gel-MOD was isolated by freezing and lyophilization (Christ freeze-dryer alpha I-5). The DS was determined using ^{1}H-NMR (Bruker Avance WH 500 MHz) using D_2O as solvent at elevated temperature (40 °C) as reported earlier resulting in a DS of 95% [25].

2.2.1.2. Development of gel-norbornene (gel-NB)

Gel-NB was synthesized following a previously reported protocol [16] (figure 1(a)). Briefly, the carboxylic acid functionalities in 5-norbornene-2-carboxylic acid were converted into an activated succinimidyl ester via reaction with EDC and NHS for 25 h, using a 1.25 molar excess of 5-norbornene-2-carboxylic acid (relative to the amount of EDC added). To this end, EDC and NHS were dissolved in a respective 1:1.5 ratio in dry DMSO under Argon atmosphere. Afterwards, the temperature was raised to 50 °C and gelatin type B was added to the reaction mixture resulting in 2 equiv. of norbornene succinimidyl ester relative to the primary amines present in gelatin (0.385 mmol g^{-1}) and allowed to react for another 20 h. Next, the mixture was precipitated in a ten-fold excess of acetone, filtered on filter paper (VWR, pore size 12–15 μm) using a Büchner filter to remove the formed urea side products and DMSO, followed by dissolving in DDW and dialysis for 24 h against distilled water (molar mass cut-off 12 000 – 14 000 g mol^{-1}). After dialysis, the reaction mixture appeared turbid as a result of the modification of the primary amines resulting in a pH close to the isoelectric point of the gelatin (i.e. 5). Therefore, the pH of the mixture was adjusted to ~7.4 using 5 M NaOH resulting in a clearing of the solution. Finally, the pure product was isolated by freezing and subsequent lyophilization. The DS was assessed using ^{1}H-NMR spectroscopy using D_2O as a solvent at 40 °C (Bruker WH 500 MHz) by comparing the norbornene double bond proton signals at 6.33 and 6.00 ppm, corresponding to the incorporated endo derivative, and at 6.28 and 6.28 ppm, corresponding to the incorporated exo equivalent [26], to the methyl signals of the side chains in valine leucine and isoleucine at 1.01 ppm as previously reported resulting in a DS of 89% [16].

2.2.1.3. Thiolation of gelatin (gel-SH)

Thiolation of the primary amines in gelatin type B was performed according to a previously reported protocol [27] (figure 1(b)). In brief, 20 g of gelatin type B (7.7 mmol reactive amines) was dissolved in 200 ml carbonate buffer (pH 10) at 40 °C. when completely dissolved, the solution was degassed and placed under inert atmosphere. Next, 0.045 g (1.5 mM) of EDTA tetrasodium tetrahydrate salt was added in order to complex any metals which can catalyze the disulfide-forming oxidation reaction. Next, 5 equiv. (relative to the primary amines of gelatin) of N-acetyl homocysteine thiolactone (38.5 mmol, 6.193 mg) were added to the reaction mixture. After addition, the reaction was allowed to proceed for 3 h under inert (Ar) atmosphere at 40 °C to prevent oxidation-induced crosslinking. The thiolated gelatin (gel-SH) was purified using dialysis (Spectra/Por molar mass cut-off 12 000–14 000 g mol^{-1}) for 24 h under inert atmosphere and the water was changed five times. After dialysis, the gel-SH was immediately frozen in liquid nitrogen and isolated via freeze drying (Christ freeze-dryer alpha I-5).

The DS was determined using an ortho-phthalic dialdehyde amine determination assay as reported earlier yielding a DS of 72% [23].

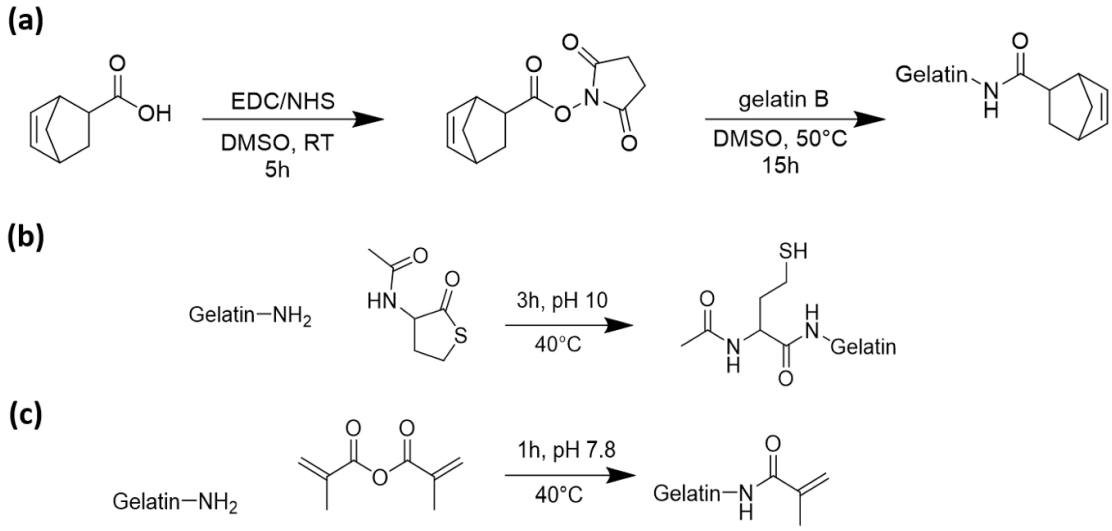

Figure 1. Different gelatin modification strategies including: (a) the formation of gel-NB using 5-norbornene-2-carboxylic acid; (b) the formation of gel-SH using n-acetyl homocysteine thiolactone; (c) and the formation of gel-MOD using methacrylic anhydride.

2.2.2. Photoinitiator synthesis (lithium (2,4,6-trimethylbenzoyl)phenylphosphinate (LAP))
The photoinitiator Li-TPO or LAP was synthesized according to a previously reported protocol [28]. The details can be found in the supporting information.

2.2.3. Physico-chemical hydrogel characterization
Different gel-NB/thiol formulations were assessed and benchmarked to gel-MOD (see table 1).

2.2.3.1. Swelling ratio and gel fraction
To determine the swelling ratio and gel fraction of hydrogel films, they were first processed into thin films using a film casting approach followed by gel-fraction and swelling ratio determination similar to a previously reported protocol [16]. The detailed experimental details can be found in the supporting information.

2.2.3.2. Rheological analysis
All rheology experiments, both *in-situ* photo-rheology and thin film rheology were performed as previously reported [16, 29]. The detailed experimental details can be found in the supporting information.

2.2.4. In vitro biological experiments
2.2.4.1. Cell culture
For the cell experiments, an hTERT immortalized human adipose-derived stem cell (hASC)/TERT1 (Evercyte GmbH, Austria) was used which was transfected with green fluorescent protein (GFP) to obtain permanently transfected green labelled cells according to a previously reported protocol [30]. Cells were cultured at 5% CO_2 at 37 °C in Endothelial Cell Growth Medium-2 (EGM-2, Lonza) supplemented with 10% foetal bovine serum (Gibco). Cells were detached with 0.5% Trypsin-EDTA upon 90% confluency.

2.2.4.2. Cell-line encapsulation experiments
For cell encapsulation experiments, GFP labelled ASCs in passage 17 or primary hASC's at passage 5 were encapsulated in 7.5 w/v% of the different thiol-ene formulations, in the presence of 2 mol% LAP (relative to the number of crosslinkable functionalities) and an equimolar thiol:ene ratio.

To this end, first 600 μl of each gelatin formulation was prepared at 10 w/v% in phosphate-buffered saline (PBS) in the presence of the photoinitiator (PI) and thiolated crosslinker. After complete dissolution, the samples were diluted with 200 μl of a stock solution containing 2 million cells ml^{-1} as counted using a Neubauer chamber resulting in a final cell density of 500 000 cells ml^{-1}. From the obtained solution, three pellets of 30 μl were pipetted in a methacrylated glass bottom dish (IBIDI) as previously described [16] followed by 10 min of UV-A irradiation (365 nm, 25 mW cm^{-2} corresponding to 15 J cm^{-2}). After crosslinking, the samples were incubated in appropriate culture medium and maintained at 37 °C in an incubator (high humidity, 5% CO_2). At different time points, the metabolic activity of the cells was measured using a Presto Blue assay and the cellular morphology was monitored using confocal laser scanning microscopy (LSM) (Zeiss, Oberkochen, Germany). The medium was replaced every other day.

2.2.4.2.1. Methacrylation of IBIDI dishes
In order to covalently attach the hydrogels to the glass of the IBIDI dishes, they were silanized with trimethoxysilylpropyl methacrylate. To this end, they were first cleaned using a plasma treatment, followed by

Table 1. Overview of the different gelatin based formulations.

Ene derivative	Gel-MOD DS 95%	Gel-NB DS 90%	Gel-NB DS 90%	Gel-NB DS 90%	Gel-NB DS 90%	Gel-NB DS 90%	Gel-NB DS 90%
Crosslinker	/	DTT	TEG2SH	PEG2SH 3400	PEG4SH 10 000	PEG4SH 20 000	Gel-SH DS 72
Gelatin concentration (w/v%)	10	10	10	10	10	10	10
Thiol-ene ratio		1	1	1	1 or 0.5	1	1
Photoinitiator	Irgacure 2959; LAP; P2CK	Irgacure 2959; LAP; P2CK	Irgacure 2959; LAP; P2CK	Irgacure 2959; LAP; P2CK	Irgacure 2959; LAP; P2CK	Irgacure 2959; LAP; P2CK	Irgacure 2959; LAP; P2CK

incubation in a solution containing trimethoxysilylpropyl methacrylate. This solution was composed of 48 ml ethanol in 50 ml of distilled water containing 0.3 ml acetic acid and 2 ml trimethoxysilylpropyl methacrylate which was stirred for 30 min. The IBIDI dishes were filled with 2 ml solution for 1 h, followed by rinsing with double distilled water and drying at 45 °C.

2.2.4.3. Presto blue metabolic activity assay

The metabolic activity was measured according to a previously described protocol [16]. The details of the experiments can be found in the supplementary information.

2.2.4.4. Dark toxicity screening

To assess the cytotoxicity of the components of the different gel-NB formulations a dark toxicity assay was performed similar to a previously described protocol [28]. The detailed experimental conditions can be found in the supporting information.

2.2.4.5. Live/dead staining

A live/dead assay using calcein-acetoxymethyl (Ca-AM) and propidium iodide (PI) was performed to assess the cell viability of encapsulated primary hASCs. To this end, a stock solution was made consisting of 2 μl Ca-AM (Sigma Aldrich) and 2 μl PI (Sigma Aldrich) for every 1 ml of PBS. In each well, 150 μl of the stock solution was added and incubated for 30 min at room temperature covered with aluminium foil. Following incubation, the solution was removed and the cells were visualized with a fluorescent microscope (Olympus IX81) equipped with a GFP and Texas Red filter. The cell images were processed through ImageJ software.

2.2.5. Processing

2.2.5.1. 2PP additive manufacturing

2PP experiments were performed on a previously reported in-house developed set-up as previously reported [16]. The experimental details can be found in the supporting information.

2.2.5.2. Multiphoton photocleaving

To assess potential cleaving of the hydrogels under the influence of two-photon absorption, an assay was performed towards the influence of laser dose on potential cleavage. To this end, a gel-NB hydrogel was crosslinked inside a methacrylated IBIDI dish in the same spacer as applied in the 2PP experiments using 2 mol% LAP in the presence of DTT in a thiol:ene ratio of 0.5 by using UVA (365 nm, 25 mW cm^{-2}) irradiation for 30 min (i.e. 15 J cm^{-2}). Next, the sample was equilibrium swollen in PBS and cut in half using a scalpel to have a clear edge [31] . Next, 'channels' (350 × 30 × 100 μm) were irradiated inside the material spanning over this 'edge' using the same setup as for the 2PP structuring by scanning both in X and Y direction with a hatch distance of 0.5 μm and Z distance of 1 μm. An array was structured with speeds varying scanning from 25–150 mm s^{-1} at a 25 mm s^{-1} increment and laser powers varying from 50 to 200 mW with a 50 mW increment. Next, the sample was incubated at 37 °C for 24 h to remove cleaved material. Finally, the samples were incubated in a solution containing FITC-dextran with a molar mass of 2000 kg mol^{-1} to visualise the channels. Next, the samples were imaged using both optical and LS microscopy.

2.2.6. Statistics

For all samples, Gaussian distribution was assumed. Statistical significance was analyzed using GraphPad InStat using a one-way analysis of variance with Bonferroni post-hoc test. The level of statistical significance was defined as $^{***}p < 0.001$, $^{**}p < 0.01$, $^{*}p < 0.05$.

3. Results and discussion

3.1. Gelatin modification

In order to obtain the photo-crosslinkable gelatin derivatives, different modification strategies were applied. Throughout the present work, gel-MOD (DS 95% (i.e. 0.36 mmol g^{-1} of gelatin) was used as a benchmark as it is a commonly used material in the field of biofabrication and TE [1, 12, 32]. The

material was obtained via reaction of the primary amines of the (hydroxy)lysine and ornithine amino acids in gelatin B with methacrylic anhydride (figure 1(c)) [11]. Gelatin type B was selected as previous work indicated that the latter exhibits superior immunocompatibility [33]. For the thiol-ene click hydrogels, the aim of the present research is to assess the influence of the applied thiolated crosslinker on the properties of gelatin thiol-ene networks. Therefore, norbornene functionalities were introduced to gelatin via reaction of the primary amines to the carboxylic acid of 5-norbornene-2-carboxylic acid using carbodiimide coupling chemistry resulting in gel-NB (DS 89% or 0.34 mmol g^{-1} of gelatin) [16] (figure 1(a)). It should be noted that during this synthesis the presence of unreacted EDC molecules should be eliminated. On the one hand, these unreacted EDC molecules can result in the formation of zero-length crosslinks between the primary amines present in the (hydroxy)lysine and ornithine and the carboxylic acids of the glutamic and aspartic acid present in gelatin [1, 29]. On the other hand, all EDC has to be reacted prior to the addition to gelatin, as the combination of a carbodiimide and an acid catalyst (5-norbornene-2-carboxylic acid) in DMSO could result in oxidation of the alcohols present in gelatin to their respective aldehyde or ketone following a Pfitzner-Mofatt-oxidation [34]. These aldehydes can also result in crosslinking via reaction with the primary amines of gelatin resulting in Schiff's base formation [1]. Norbornene was selected as the 'ene' functionality due to its high reactivity and the fact that it is not susceptible to competitive thiol-Michael addition since this reaction can already occur at mild basic conditions (i.e. physiological conditions) and could result in undesirable crosslinking of the entire sample during the 2PP processing [15, 35].

Gel-SH was obtained via the reaction of the primary amines present in gelatin with N-acetyl-homocysteine thiolactone using a previously reported protocol (figure 1(b)) [27].

3.2. Influence of thiolated crosslinker on physico-chemical properties of gelatin hydrogels

The assessed thiolated crosslinkers are depicted in figure 2(a) and table 1 and include gel-SH (DS 72%), DTT, TEG2SH, PEG dithiol with a molar mass of 3400 g mol^{-1} (PEG2SH 3400), PEG4SH with a molar mass of either 10 000 g mol^{-1} (PEG4SH 10 000) or 20 000 g mol^{-1} (PEG4SH 20 000). DTT was selected as it is a crosslinker which is often exploited in the framework of thiol/ene systems [16, 18, 36–38]. Besides DTT, also different thiolated PEG derivatives were selected, differing in molar mass (i.e. 220–20 000 g mol^{-1}) and/or number of thiols per crosslinker (i.e. 2 or 4) as some PEG-based thiolated crosslinkers have already been reported in literature [1, 18, 39, 40]. However, there has been very little research on the comparison of different (PEG-based) crosslinkers. The use of different PEG-based crosslinkers allows to screen towards specific effects of molar mass and number of thiols on the physico-chemical properties of the crosslinked hydrogel without changing the chemical functionalities. Finally, a thiolated gelatin was also selected as this will result in a network without the incorporation of any synthetic, non-degradable macromolecular species while also exhibiting a relatively high number of thiols per crosslinker molecule (i.e. ± 14 thiols per gelatin chain). Therefore, it could potentially result in a stiffer hydrogel network. Despite these potential beneficial aspects, there are very few reports in literature using thiolated gelatin as crosslinker for 'ene'-functionalized gelatins [23, 41, 42].

Additionally, it should be noted that other strategies to influence the network properties can consist of varying the total gelatin concentration in the formulation [1, 16, 29]. However, it is known that changing the gelatin concentration can have a significant influence on cellular behaviour [1, 40, 43]. Taking this into account, all hydrogel formulations were prepared using a 10 w/v% total gelatin concentration in a thiol-ene ratio of 1 (unless stated otherwise).

Another strategy to influence the hydrogel properties in thiol-ene hydrogels is altering the thiol-ene ratio. In this respect, the hydrogel properties can be tuned while keeping the gelatin concentration constant [16, 40]. Although outside the main scope of the current work, this effect was also investigated for the gel-NB PEG4SH 10 000 formulation. To this end, besides altering the thiol-ene ratio, also experiments were performed for which the total polymer concentration (i.e. gel-NB + PEG4SH 10 000) was kept at 10 w/v % to have a more comparable total polymer fraction (see supporting information 3.2 and figure S1) (is available online at stacks.iop.org/BF/13/015017/mmedia).

3.3. Influence of the applied photoinitiator and crosslinker on the crosslinking kinetics

A first characteristic to compare different photo-crosslinkable systems includes the crosslinking kinetics. To this end, photo-rheology was performed using either 2 mol% (relative to the number of 'ene' functionalities) LAP (figure 2(b)) or Irgacure 2959 (figure 2(c)) as PI. When monitoring the storage modulus (G′) over time, the difference in reactivity between the thiol-ene step-growth systems and the conventional chain-growth gel-MOD system is apparent. The latter being characterized by a lag phase upon UV irradiation. This lag phase is a consequence of oxygen inhibition during the reaction. Before the polymerization is initiated, the oxygen has to be consumed first by the radicals, which is not the case for the step-growth thiol-ene systems, resulting in the observed faster crosslinking reaction [44].

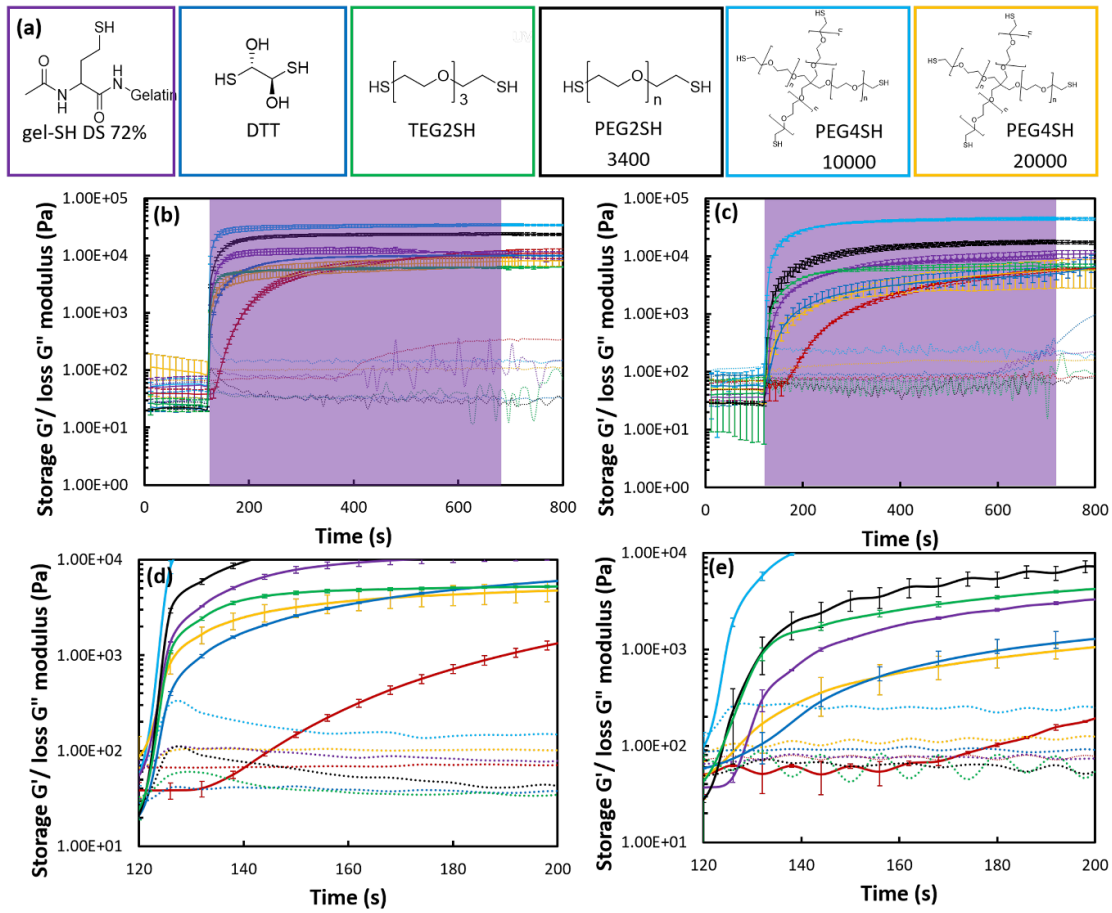

Figure 2. (a) Overview of the different applied thiolated-crosslinkers; *In-situ* photo-rheology of the different thiol-ene formulations with a 1:1 thiol-ene ratio using gel-MOD DS 95% as reference in the presence of (b) LAP or (c) Irgacure 2959 as PI (d) and (e) zoomed in regions of the crossover point in the presence of LAP or Irgacure 2959.

Table 2. Comparison between gel-points obtained for crosslinking of the different hydrogel formulations.

Gel Point	Gel-MOD (s)	DTT (s)	PEG4SH 20k (s)	Gel-SH (s)	TEG2SH (s)	PEG2SH (s)	PEG4SH 10k (s)
LAP	19.9 ± 1.47	0.36 ± 0.01	0.16 ± 0.22	0.19 ± 0.05	0.14 ± 0.03	0.04 ± 0.01	0.03 ± 0.01
Irgacure	49.5 ± 3.54	9.18 ± 1.87	7.35 ± 1.69	4.57 ± 3.62	0.62 ± 0.09	0.55 ± 0.17	0.1 ± 0.05

Furthermore, crosslinking typically occurs faster in the presence of LAP (figure 2(b)) in comparison to the more conventional Irgacure 2959 (figure 2(c)). This is reflected more quantitatively by assessing the gel points or crossover points between the storage (G′) and loss (G″) moduli that indicate the transition from predominantly viscous to elastic behaviour for the different formulations [45] (figures 2(d), (e) and table 2). The difference in reactivity between both PIs is especially apparent for the gel-MOD derivative as this is characterized by slower reaction kinetics in comparison to the thiol-ene systems [16]. This is a consequence of the higher efficiency of LAP in the UV-A region as it is characterized by a molar absorptivity at 365 nm of 218 M^{-1} cm^{-1} [39] vs 4 M^{-1} cm^{-1} [32] for Irgacure 2959. This means that for LAP, more radicals will be formed upon UV irradiation. Since high radical concentrations can compensate for the oxygen inhibition effect due to the rapid oxygen consumption, this results in shorter lag times and concomitantly, faster gel points are observed [1, 46]. However, the difference in reactivity between both PIs is not significant for gel-SH, TEG2SH, PEG2SH and PEG4SH 10 000 due to the spring loaded behaviour of the thiol-norbornene reaction, and the absence of oxygen inhibition. When comparing the kinetics of the different formulations, the differences in gel point between the different thiol-ene systems are minor (table 2).

Additionally, no significant difference in storage modulus (G′) in the relaxed state with respect to gel-MOD is observed after 10 min crosslinking for most thiol-ene formulations (i.e. 6–10 kPa when using LAP and 5–11 kPa when using Irgacure 2959 as PI) with

the exception of PEG2SH 3400 (i.e. 17 500 ± 1100 Pa for Irgacure 2959 and 23 950 ± 1200 Pa for LAP) and PEG4SH 10 000 (i.e. 44 600 ± 2000 Pa for Irgacure 2959 and 34 550 ± 1400 Pa for LAP) which outperform the conventional gel-MOD derivative, while PEG4SH 10 000 is even outperforming all evaluated crosslinkers in terms of mechanical properties. Furthermore, the thiol-ene systems already obtain their final mechanical properties after ±60 s crosslinking, whereas gel-MOD requires 10 min to reach similar storage moduli.

3.4. Influence of the applied crosslinker on the mechanical properties of the hydrogel at equilibrium swelling

During *in situ* photo-rheology, the mechanical properties of a hydrogel in relaxed state are obtained, which is less relevant when considering the final application in hydrated state. Therefore, a second assay was performed during which the rheological properties of equilibrium-swollen, crosslinked hydrogel films at physiological conditions were assessed along with their swelling ratio (figure 3). In a first experiment, the films were crosslinked using either Irgacure 2959 or LAP from solution immediately after film casting. Under these circumstances, generally higher storage moduli are obtained when using LAP as PI. This effect is related to the higher efficiency of the PI around 365 nm on the one hand while on the other hand, the acylphosphinate functionality in LAP will cleave upon activation which results in the loss of the light-absorbing chromophore [45]. As a consequence, a larger penetration depth of UV-light during crosslinking is ensured, which is not the case for Irgacure 2959 [45]. This is further substantiated by the swelling ratio of the gels as in general, lower swelling ratios are obtained for the hydrogels which were crosslinked in the presence of LAP (figure 3(b)).

It is generally known that chain-growth hydrogels (i.e. gel-MOD) typically exhibit a higher stiffness due to the presence of kinetic chains resulting in the linking of different functionalities in the same junction knot [14]. The presence of these non-degradable kinetic chains was further exemplified via Gel permeation Chromatography (GPC) analysis on crosslinked samples which were hydrolysed using HCl (see supporting in formation 3.4, figure S2 and table S1) [14]. It was shown that these non-degradable kinetic chains exhibited a Mn of around 5 kg mol^{-1} (see table S1). For thiol-ene systems this is not the case, as the number of functionalities linked in one junction knot depends on the number and relative distance between the thiols on the crosslinker molecule due to the reaction of complementary functionalities [1, 16].

Furthermore, in case of chain-growth hydrogels, several methacrylate functionalities on the same gelatin chain can react with each other, resulting in primary cycles and associated network imperfections [47]. This effect is less pronounced for the thiol-ene systems due to the orthogonal crosslinking occurring between complementary functionalities of gelatin and the applied thiolated crosslinker. However, it should be noted that while no non-degradable kinetic chains are formed in thiol-ene hydrogels, the use of non-degradable PEG-based crosslinkers will also result in non-degradable polymer residues (see supporting information 3.4; figure S2 and table S1). Here, it was shown that especially for the PEG4SH 10 000 crosslinker, larger polydispersities were obtained. This indicates that despite the orthogonal reaction, also a suboptimal network is obtained for the PEG4SH as a consequence of competitive disulphide formation. This effect is most pronounced for gel4SH 10 000 as the higher total polymer concentration requires longer dissolution times at increased temperature which will accelerate this unfavourable side reaction [48]. Although this is a disadvantage from a network perspective, it is anticipated that the obtained non-degradable PEG-residues will not pose any problems upon degradation *in vivo* as they exhibit low molar masses (i.e. <30 kDa) which can be secreted through the kidneys [49]. Finally, it should be noted that the gel-NB/gel-SH formulation and the gel-NB/DTT formulations are the only formulations which can be fully degraded into small molecules (see figure S2).

The present research indicates that the applied thiolated crosslinker has a substantial influence on the final mechanical properties as previously reported by Munoz *et al* [18]. In the present work, the highest storage modulus was observed when PEG4SH 10 000 was applied as crosslinker which is a consequence of the following aspects (figure 3(a)). First, the crosslinker contains four thiol functionalities, resulting in the coupling of four norbornene functionalities in one junction knot. The other applied crosslinkers, with the exception of gel-SH and PEG4SH 20 000, only exhibit two functionalities, thereby resulting in a less densely crosslinked network, as also reflected by the higher swelling ratio (figure 3(b)). However, both PEG2SH 3400 and PEG4SH 10 000 exhibit superior mechanical properties compared to the hydrogels crosslinked using gel-SH which contains approximately 14 thiol groups/crosslinker. This is a consequence of the fact that all systems were crosslinked in a 1:1 thiol/ene ratio while keeping the total gelatin concentration at 10 w/v%. Since changing the gelatin content would also result in a variation of the amount of RGD functionalities which can influence the biological response, irrespective of the applied crosslinker [40]. This means that for gel-NB/gel-SH, the total polymer concentration was 10 w/v% while all other formulations contain 10 w/v% gel-NB, for gel-NB/PEG2SH 3400, the addition of an equimolar amount of thiols resulted in a total polymer concentration of ±16 w/v% (i.e. 10 w/v% gel-NB and 6 w/v%

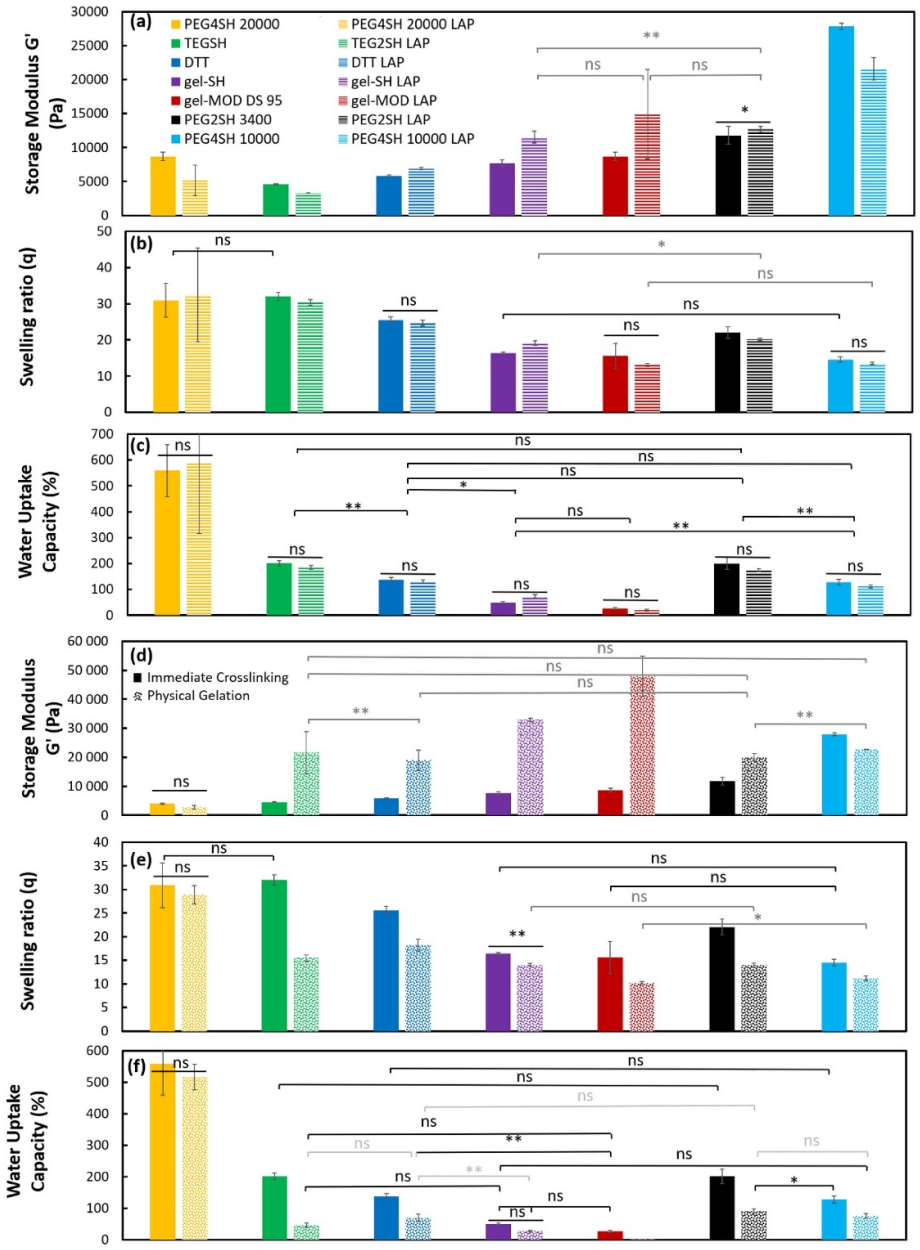

Figure 3. (a) Influence of PI on storage modulus and (b) associated swelling ratio and (c) water uptake capacity relative to the relaxed state. The full bars represent hydrogels crosslinked using Irgacure 2959 and the dashed bars were crosslinked using LAP. Influence of physical gelation prior to crosslinking using Irgacure 2959 on (d) storage modulus and (e) swelling ratio and (f) water uptake capacity relative to the relaxed state with the full bars crosslinked from solution and the dotted bars after a 1 h incubation period at 4 °C to induce physical crosslinking prior to UV irradiation. All statistical differences are significant with $p < 0.001$ unless stated differently with $^{**}p < 0.001$, $^{*}p < 0.05$ and ns indicating no statistical significance.

PEG2SH 3400) and for gel-NB/PEG4SH 10 000, this was ±18.5 w/v% (i.e. 10 w/v% gel-NB and 10 w/v% PEG4SH) resulting in the observed superior mechanical properties. In this respect, it should be noted that the lower swelling ratio for these samples containing macromolecular crosslinkers is a consequence of a higher polymer concentration, and therefore higher dry mass after freeze drying of the sample, which could lead to wrong conclusions. Therefore, a better measure to compare samples with a different total polymer concentration, especially when looking at shape fidelity in 3D printing is the water uptake capacity (figure 3(c)). This value is calculated as the additional water uptake immediately after crosslinking (i.e. relative to the polymer + water content in the relaxed state). A first important observation here is the fact that no significant differences in water uptake capacity are observed when using LAP vs Irgacure 2959 (figure 3(c)), which is intuitive as the initiation efficiency should not influence the network properties, especially when exploiting orthogonal crosslinking chemistry. When looking at the water uptake capacity, the results are more intuitive in comparison to the swelling ratio with the gel-NB/gel-SH formulation exhibiting the lowest water uptake capacity as this is the crosslinker with the highest amount of thiols (i.e. ± 14) per molecule. The second most dense network is obtained when using the 4-arm

PEG4SH 10 000, whereas, the next one is the gel-NB/DTT formulation, which contains the shortest bifunctional thiolated crosslinker. It is clear that the hydrophilic PEG-based crosslinkers result in higher water uptake capacities. Despite the use of these low molar mass crosslinkers, the mechanical properties are poorer in comparison to the higher molar mass PEG2SH 3400 (i.e. 3.3–6.8 kPa vs 11–12 kPa). This can possibly be attributed to competitive disulphide formation for TEG2SH, since the GPC results of the non-degradable residues indicates a considerably higher molar mass for TEGSH as anticipated (i.e. 2005 g mol^{-1} vs 226 g mol^{-1}). Furthermore, also the higher total polymer concentration in the PEG-containing hydrogels will play a role. However, when preparing gel-NB/PEG4SH at a total polymer concentration of 10 w/v% (i.e. ± 6 w/v% gel-NB and ±4 w/v % PEG4SH 10 000), a hydrogel is obtained with a comparable storage modulus to gel-MOD (i.e. 13.2 kPA vs 14.8 kPa). This storage modulus is also comparable to the storage modulus of gel-NB/gel-SH (i.e. 11.5 kPa) (figures 3(a) and S1(b)). Finally, it should be noted that based upon this reasoning, superior mechanical properties are anticipated for PEG4SH 20 000, which in practice results in the weakest gels. This might be due to the larger distance between the thiols on the one hand and phase separation phenomena occurring between gelatin and PEG, resulting in a heterogeneous mixture and concomitant poor network formation. This hypothesis was substantiated by a lower gel fraction (i.e. all hydrogels exhibited similar gel fractions of > 85% with the exception of PEG4SH 20 000 around 70% (data not shown)) and during 2PP experiments (section 3.6).

Despite the fact that a multifunctional, branched, thiolated crosslinker results in similar or higher storage moduli compared to gel-MOD, the latter are characterized by the lowest swelling ratio (figures 3(a) and (b)). This is in line with previous reports from literature [14, 23]. In this respect, the gel-MOD hydrogels are characterized by the presence of hydrophobic kinetic oligo-methacrylamide chains, as also shown by GPC analysis, which also result in a lower water uptake capacity [18] (see figure S2 and table S1).

The swelling ratio can be an important aspect of a hydrogel in the framework of AM. This is especially relevant when using high resolution technologies, as post-production swelling of the material can result in deviations from the applied computer-aided design (CAD) [29, 50].

Based on the rheological and water uptake capacity results, it can be concluded that in general, the mechanical properties improve and the swelling ratio decreases when increasing the number of thiols present on the thiolated crosslinker. Furthermore, the mechanical properties of the hydrogels improve upon increasing the molar mass of the applied crosslinker. However, this is partially due to the relative increase in polymer concentration (i.e. gelatin + crosslinker), thereby resulting in a denser hydrogel.

3.5. Influence of physical interactions on mechanical properties and swelling ratio of the obtained hydrogels

A second important aspect when applying gelatin for biofabrication application is its physical gelation. Certain AM techniques either require or benefit from this physical gelation behaviour to enable the generation of 3D structures prior to covalent crosslinking [1]. For example, deposition-based techniques often apply this physical gelation behaviour to lock the deposited structure prior to chemical crosslinking [51–53]. Additionally, in case of 2PP-processing, the presence of a physical gel can be beneficial as it provides mechanical support to the formed structure, which enables the construction of more complicated architectures [1, 23, 51]. Furthermore, it is known that the formation of a physical gel can have an influence on the network properties [1]. When a material is crosslinked in a physical gel state, this can result in a stiffer network with a lower swelling ratio, as the physical gelation occurs due to the formation of triple helices via interchain hydrogen bonding between the proline and hydroxyproline present in the gelatin backbone [6, 8]. As a result, semi-crystalline junction zones are formed, which can result in a proximity effect of the crosslinkable functionalities thereby resulting in a higher crosslink efficiency. On the other hand, these semi-crystalline junction zones can partially be 'Frozen/locked' via the introduction of chemical bonds [29, 54]. As a consequence of both aspects, in general, a denser hydrogel network is formed with superior mechanical properties. This aspect is beneficial when using a solution containing only gelatin. However, when other polymers are introduced into the formulation, these supramolecular interactions can result in phase separation between the components thereby resulting in inhomogeneous networks [4, 55]. Thiol/ene systems typically require a thiolated (polymeric) crosslinker, which could induce phase separation during physical gelation. Therefore, the effect of physical gelation prior to crosslinking was assessed for the different formulations. To this end, hydrogel films were prepared using 2 mol% Irgacure 2959 as PI either via direct UV-induced crosslinking after film casting (figures 3(c) and (d) full bars) or following a 1 h physical gelation period at 4 °C, prior to UV irradiation (figures 3(c) and (d) dotted bars). In general, a similar trend is witnessed for all formulations as an increase in stiffness in combination with a decrease in water uptake capacity can be observed for the hydrogels which were physically gelled prior to UV crosslinking (figures 3(d) and (f)). The effect is most pronounced for the chain-growth gel-MOD, which outperforms all other formulations both in terms of stiffness and water uptake capacity with a 5.5-fold increase in stiffness while

being almost completely precluded from swelling (i.e. 0.2%) compared to the gels obtained after crosslinking from solution (i.e. 10.2%). This was anticipated as no phase separation can occur in this system while the proximity effect of the methacrylamides due to triple helix formation also decreases the probability towards the formation of primary cycles resulting in network imperfections. Due to the structural similarity between gel-NB and gel-SH, it is no surprise this formulation results in the second stiffest hydrogel with a 4.3-fold increase in storage modulus and a 1.8-fold decrease in water uptake capacity. Furthermore, also for the low molar mass crosslinkers (i.e. DTT and TEG2SH) this effect is significant, as their small molecular size (i.e. 154 g mol^{-1} and 226 g mol^{-1}) and low concentration will not interfere substantially with the triple helix formation. As anticipated, the lowest benefit exists for the high molar mass crosslinkers (i.e. PEG-based) whereas the 4-arm PEG crosslinkers even result in a slight decrease in mechanical properties when first inducing physical gelation due to phase separation occurring between the high molar mass components.

Consequently, the use of gel-SH as crosslinker results in the most homogeneous network as no synthetic crosslinkers are incorporated in the hydrogel, therefore no non-biodegradable polymer chains are present (figure S2), which forms the closest mimic of the conventional gel-MOD hydrogel system in terms of swelling ratio and mechanical properties, with the benefit of the characteristic fast thiol-ene reaction kinetics and full biodegradability.

3.6. Influence of applied crosslinker on 2PP processing performance

To assess the processability differences of the discussed hydrogel formulations, a 2PP structuring threshold and swelling assay was performed in line with previously reported assays [16, 29, 56]. In this assay, cubes of 100 μm × 100 μm × 100 μm were structured at different laser powers with a constant scanning speed of 100 mm s^{-1} on top of a methacrylated glass slide (figure 4(a)). As a result, an overview of the processing window of each formulation becomes apparent, while measuring of the top surface of the cube by measuring the highest, non-distorted slice in the confocal Z-stack still resembling a cube, which is not limited in swelling by adhesion to the glass, provides an indication of the swelling degree, and therefore the reproducibility between CAD design and final structure (figure 4(b)). In addition, it also provides insights in the crosslink density, as from a certain laser power onwards, no further decrease in swelling is anticipated, thereby evidencing a fully crosslinked network [16].

The polymerization threshold for the different thiol-ene formulations is similar and extremely low (i.e. 4–5 mW average laser power), which is a 20-fold decrease in comparison to the conventional gel-MOD hydrogels (i.e. 80–90 mW average laser power). An exception in this respect are the PEG4SH 20 000 and gel-SH (figure 4). For the PEG4SH 20 000, the structuring threshold was observed at 20 mW. Although this is still significantly lower compared to the threshold of conventional gel-MOD (i.e. 90 mW), the swelling profile as a function of increasing laser powers appears quite random and is substantially higher compared to the other thiol-ene formulations. Additionally, it became apparent that phase separation between gel-NB and PEG4SH 20 000 occurred as evidenced by the presence of spherical-shaped particles. This is further substantiated by the high amount of debris that can be observed on the LSM images after structuring (figures 4(a) and S3). The assay indicated the far superior processability of the thiol- ene hydrogels over the conventional chain-growth hydrogels.

Furthermore, when considering the swelling behaviour of the top surface of the cubes in the different formulations, a plateau in swelling occurs around an average laser power of ± 10 mW for the thiol-ene systems. This is an indication of the presence of a fully crosslinked network, in contrast with the gel-MOD hydrogel that exhibits a clear laser power dependency within the presented range which was also previously reported [29, 56].

When the laser power is further increased, this plateau is maintained initially as expected, but at higher laser powers (i.e. above 30–40 mW), the swelling increases again. This behavior can be attributed to some extent to the formation of a larger voxel with increasing laser powers [57, 58]. However, these effects are considered to be of a lower order of magnitude as observed in the present experiments and would not result in deformations of the basic cubic structure [59]. Furthermore, when observing the shape of the cubes (figures 4–5 and S3), another phenomenon is clearly responsible for this effect at high laser powers. Indeed, instead of a gradual increase in swelling when moving away from the glass in the Z-direction as observed at lower laser powers and as previously reported [16, 29], the swelling appears to reach a maximum first and then decreases again with increasing height (figure 5) (table 3). Therefore, besides measuring the top surface, also the maximum swelling for each cube was assessed. This reflected the increase in volume with increasing laser powers even more (figure 4(c)). A similar trend was also previously reported by Dobos *et al*, who observed a similar effect in the mechanical properties of the obtained structures [19, 24]. Since the swelling is larger halfway up the structure and decreases again, it is anticipated that this swelling effect is present due to a competitive photocleavage reaction. It is hypothesized that this photocleavage occurs in the amide bonds of the gelatin backbone as amide bond photo-degradation has been reported, especially in aqueous environments [60–62].

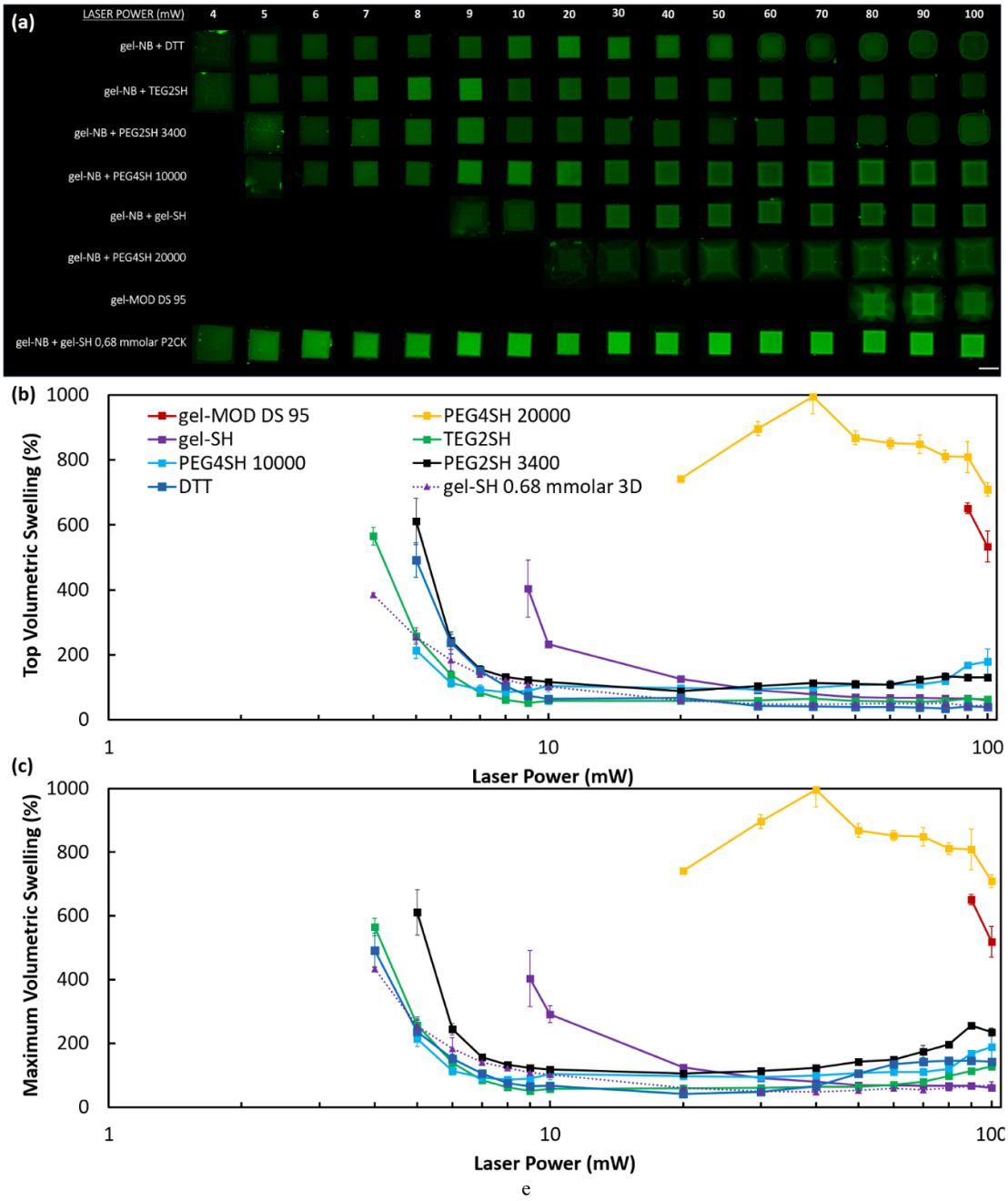

Figure 4. (a) Overview of 2PP processing range at 100 mm s^{-1} scanning speed in terms of laser power by structuring 100 × 100 × 100 μm^3 cubes in the different formulations. (Scale bar represents 100 μm) (b) Volumetric swelling calculated from the comparison of the top surface area to the applied CAD in panel A; (c) Maximum volumetric swelling calculated from the surface area of the layer with the highest swelling degree relative to the applied CAD model in panel (a).

Additionally, literature states that the photo-lysis or photo-oxidation induced degradation of the amide bond in nylon occurs following a free-radical reaction [61]. These effects typically require very long times (i.e. weeks to months) in single photon experiments. However, in the present set up, very high laser light intensities are applied, resulting in the formation of a very high number of radicals, especially at high average laser powers (figure S4). This cleaving-effect is especially anticipated since there exists some overlap of the different voxels in between the different layers (figure 6).

This further confirms the observations in sections 3.2–3.4. Due to these reproducibility issues, no further characterization experiments were performed using this formulation. For the gel-NB/gel-SH hydrogels, it should be noted that all hydrogels were crosslinked in the presence of 2 mol% P2CK as PI calculated relative to the number of norbornene/methacrylamide functionalities, thereby corresponding to 0.68 mM of PI for most formulations. However, for the gel-NB/gel-SH formulations, the total amount of gelatin was kept at 10 w/v% while maintaining a 1:1 thiol:ene ratio. Therefore, the

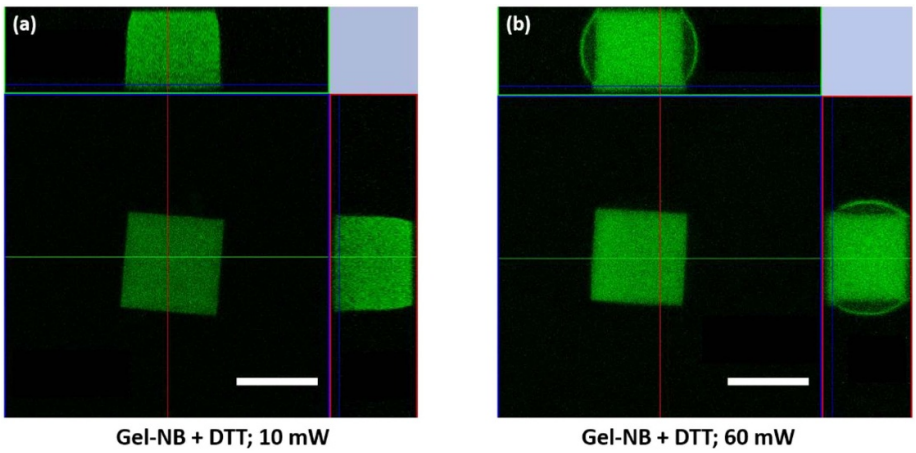

Figure 5. (a) Orthogonal projection of the structured cubes indicating the anticipated swelling profile as observed at low laser powers (b)and the deviations from this behavior at high laser powers. (Scale bars represent 100 μm).

absolute PI concentration was lower as it was adjusted with respect to the amount of norbornene functionalities (i.e. 0.3 mM), resulting in a higher polymerization threshold and a higher energy dose before reaching a plateau value. To provide a fair comparison, an additional experiment was performed where this formulation was processed in the presence of 0.68 mM PI, thereby resulting in a comparable polymerization threshold to the other thiol/ene systems (i.e. around 4 mW average laser power) (figure 4).

To quantify this overlap to some extent, the voxel dimensions can be calculated using the following formulas [59]:

$$\omega_{xy} = \frac{0.325\,\lambda}{\sqrt{2}\,\mathrm{NA}^{0.91}}\,(\text{if NA} > 0.7) \qquad (1)$$

$$\omega_z = \frac{0.532\,\lambda}{\sqrt{2}}\left(\frac{1}{n - \sqrt{n^2 - \mathrm{NA}^2}}\right) \qquad (2)$$

With ω_{xy} being the $1/e$ width intensity squared profile of a Gaussian function in the XY-plane and ω_z the $1/e$ width of the Gaussian function along the Z-axis; λ the applied wavelength (i.e. 800 nm); NA the numerical aperture of the objective (i.e. 0.85) and n the refractive index, which is estimated to be around 1.35 based on previous measurements (data not shown) and the high dilution of the hydrogel precursors in the solution. As a consequence, the voxel has an XY-diameter equaling two times the $(1/e^2)$ radius or $= 2\sqrt{2} \times \omega_{xy}$ (i.e. 602 nm) and a Z-length of $2\sqrt{2} \times \omega_z$ (i.e. 2826 nm) [59]. To assess how many times every voxel is exposed to the laser, these theoretical values can be compared to the applied hatching (scanned line spacing in the XY-plane) (i.e. 500 nm) and slicing distance (layer spacing in Z direction) (i.e. 1000 nm) and the fact that every layer is hatched in both X- and Y-direction to ensure proper contact between all lines. Consequently, every crosslinked voxel is exposed twice during the writing of a single layer. Furthermore, this voxel is exposed a third and a fourth time during the writing of the subsequent layer and partially exposed a fifth and sixth time during writing of the third layer since the slicing distance was set about 2.8 times lower in comparison to the intensity maximum of the illumination point spread function^2 (IPSF^2) (figure 6).

It should be noted that this overlap between the voxels of consecutive layers is performed deliberately to ensure proper attachment between the different layers as the voxel shape, as defined by the IPSF^2, can be approximated by a three-dimensional Gaussian volume resulting in smaller thicknesses towards the Z-edges [59]. As a consequence, every structured voxel is $5 \times 2 = 10$ times (partially) exposed (5 consecutive layers, 2 times per layer due to X and Y hatching) to the laser in the bulk of the structure. However, the top layers, are only (partially) exposed 6 times (i.e. two times partially during the n−2 layer at lower intensity and two times during the previous n−1 layer and two times in the center of the focal spot during the writing of the layer itself), whereas there will be 1.8 additional layers above only exposed 1.8 times to the edge of the voxel. Therefore, the observed decrease in swelling properties towards the top of the structure is consistent with partial cleavage of the bulk of the material (figure 5).

To further substantiate this hypothesis, the effect of the laser irradiation on the hydrogel material was assessed by exposing UV-crosslinked hydrogel pellets to femtosecond laser pulses similar to a previously reported protocol [31]. To this end, first, a hydrogel pellet was obtained via crosslinking of a gel-NB/DTT solution on top of a methacrylated glass slide using UV-A irradiation in the presence of LAP as PI. Next, part of the pellet was cut with a scalpel and removed resulting in a clear edge (figure S5). This edge was exposed to different laser intensities (i.e. 50–200 mW average power) at different scanning

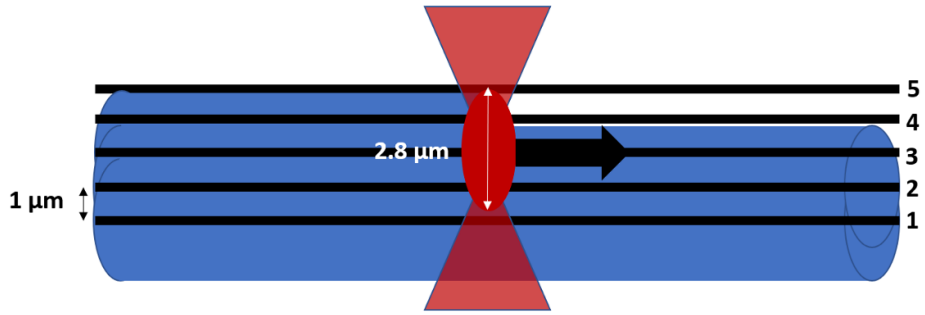

Figure 6. Schematic representation on how a voxel, which is scanned during the structuring of layer 3 will result in partial irradiation of the already structured layer 1 and 2 and layer 4 and 5 which still need to be polymerized.

speeds (i.e. 25–150 mm s^{-1}) using the same hatching parameters as applied throughout the structuring experiments in an attempt to generate channels (350 μm × 30 μm × 100 μm) over the edge of the hydrogel (figure S5). For this experiment, pellets were made starting from the DTT-containing formulation as the effect was mostly pronounced for this condition (figure 4(a)). During structuring, the samples were monitored to assess bubble formation as an indication of cleavage due to thermal effects. Next, the hydrogels were incubated in PBS at 37 °C to remove any degraded material, followed by incubation in a solution containing a highly fluorescent FITC-dextran with a molar mass of 2000 kg mol^{-1}, which cannot diffuse into the bulk of the hydrogel due to its high molar mass, but should be able to penetrate into any introduced channels in case of full cleavage (figure S5). Brightfield microscopy (figure 7) already allowed to visualize some of the exposed regions as a consequence of a difference in refractive index due to partial degradation of the material. As a result a less densely crosslinked network and concomitant decrease in refractive index is more apparent at higher spatiotemporal irradiation doses (i.e. low scanning speed (<100 mm s^{-1}) and high intensities (>100 mW)).

Furthermore, when looking at the associated LSM images (figure 7), the FITC-dextran could clearly penetrate the channels at 25 and at 50 mm s^{-1} scanning speed at high laser intensities (i.e. 150 and 200 mW average power) and at 75 mm s^{-1} at 200 mW. However, it should be noted that at 25 mm s^{-1} and 200 mW some bubble formation was observed during structuring which is a clear indication of (partial) cleavage by thermal effects, which was not the case at the higher writing speeds and/or when applying lower laser powers. The fact that not all channels could be penetrated by the fluorescent FITC-dextran, while being visible on bright field microscopy images indicates that at lower doses, the cleavage is not complete as only part of the bonds will be broken resulting in increased swelling. Furthermore, the observed difference in refractive index cannot be attributed to additional polymerization, as it is known that during the UV polymerization of gel-NB/DTT hydrogels, full conversion is obtained [16]. Additionally, it should also be noted that during this control experiment, full cleavage only occurred at lower speeds and higher intensities than during the actual structuring experiment. However, since at similar conditions and lower spatiotemporal energy doses, the channels are still visible, there will still be some competitive photo-degradation during the structuring itself, especially at higher powers, resulting in the observed peculiar swelling profile (figure 4). In this respect, the analysis of the maximum swelling relative to the applied CAD, indicates that this effect is more pronounced in hydrogels crosslinked with the bifunctional crosslinkers (i.e. DTT, TEG2SH and PEG2SH 3400) (figures 4(c), 5, S3 and table 3). This is intuitive, as in these hydrogels, a less densely crosslinked network is obtained as discussed in section 3.4. Therefore, only one amide bond in the backbone needs to be broken in between two norbornene functionalities to fully cleave this crosslink whereas in the gels with PEG4SH 10 000, at least three bonds need to be broken to realize the same effect. Consequently, this effect is less pronounced in the gels crosslinked with the PEG4SH 10 000 although a higher volumetric swelling is obtained at 100 mW in comparison to the low molar mass crosslinkers (table 3). Furthermore, the effect appears most pronounced when using PEG2SH 3400, because of the highly hydrophilic nature of PEG. After cleavage of some bonds, a less densely crosslinked network is obtained that will result in a larger additional water uptake in comparison to the low molar mass crosslinkers. This phenomenon is a consequence of the larger distance between the different thiol-ene-crosslinks (see table 3). When comparing this to the minimal volumetric swelling, a 2.1-fold increase in swelling due to photocleavage effects for PEG4SH 10 000 vs a 3.8-fold increase for DTT and a 3.4-fold increase for the TEG2SH crosslinker is observed. This effect is lacking when using the highly functionalized gel-SH which exhibits around 0.27 mmol of thiols/g gelatin or ±14 thiols per gelatin chain. The effect of cleavage is not observed in this system, because full

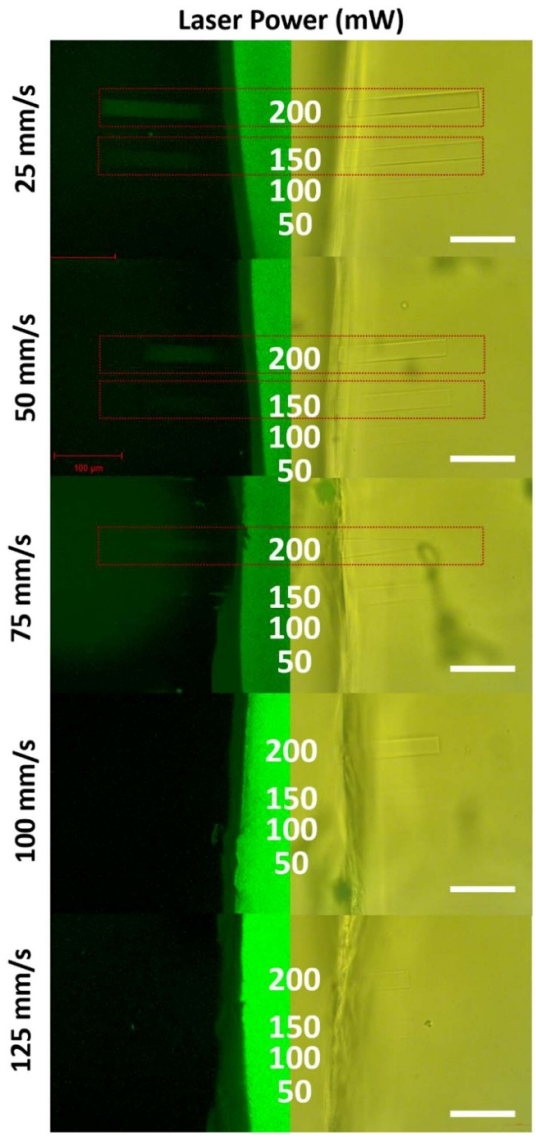

Figure 7. Laser scanning microscopy (left) and Brightfield (right) images of the 2PP-induced photocleavage of a gel-NB + DTT hydrogel as a function of laser scanning speed and average laser power in the presence of FITC-dextran 2000 kDa. The doses for which full hydrogel cleavage occurred as evidenced by penetration of the dye into the hydrogel are presented through a red square. The brightfield images show the weakening of the hydrogel as a consequence of partial cleavage resulting in a difference in refractive index due to a looser network. (Scale bars represent 100 μm).

cleavage of one 'junction zone' in the network is only obtained by cleaving a substantially higher number of bonds. For the conventional chain-growth hydrogels (i.e. gel-MOD), the reasoning is similar. Upon crosslinking, kinetic non-biodegradable chains are formed which link multiple photo-crosslinkable functionalities into one junction zone.

As a result, multiple bonds need to be broken to result in an observable cleavage of the network [14, 16, 63]. Additionally, the photopolymerization of methacrylamides is characterized by slower crosslinking kinetics (figure 2), therefore, both competitive effects will occur simultaneously, with the polymerization reaction occurring more than the cleavage

Table 3. Comparison of volumetric swelling at 100 mW average power and minimum swelling of different thiol-ene systems.

Crosslinker	Volumetric swelling @ 100 mW (%)	Minimum swelling	Molar mass between crosslinks (g mol^{-1})
PEG4SH 10 000	180 ± 40%	85 ± 10% (@ 8 mW)	2500
DTT	145.7 ± 3.1%	38.3 ± 0.5 (@ 10 mW)	226
TEG2SH	128.2 ± 10.33%	38.1 ± 4.3 (@ 20 mW)	154

thereby resulting in a decrease in swelling with increasing powers. For thiol-ene systems in contrast, full crosslinking already occurs at low laser powers (i.e. ± 20–30 mW) where further increasing the laser power will only result in more photo-cleavage as it is no longer compensated for by concurrent polymerization reactions.

Producing high-resolution self-supporting complex 3D architectures using soft materials such as hydrogels is a huge challenge in AM. Therefore an experiment was performed where a complex self-supporting structure with fine features (i.e. the Atomium) was printed as a POC experiment in the different formulations (figure 8). First, it is clear that under these fast processing conditions (i.e. 100 mm s^{-1}), the reactivity of the gel-MOD is insufficient to result in a sufficiently mechanically robust material, as the structure collapsed after development. Second, when observing the formulations with the different crosslinkers, it is clear that the post processing swelling increases with the inclusion of the more hydrophilic PEG-based crosslinkers, which is in line with the volumetric swelling assay (figure 4).

Finally, it should be noted that the lowest swelling degree and associated best shape fidelity is obtained when using the highly functional gel-SH, as also indicated in the cube swelling assay (figure 4) and UV crosslinking experiments (figure 3). rendering it the most suitable crosslinkable system for 2PP processing.

3.7. In vitro cell viability

3.7.1. Cell encapsulation experiments

Another important feature of a hydrogel formulation for TE and biofabrication applications is its biological performance. In particular, the performance of the material in the presence of cells is of paramount importance if used as a bioink (i.e. in the presence of cells during processing) or bioink component [64]. Therefore, cell encapsulation experiments as well as toxicity screening of the different components of the formulations was performed. It should be noted that due to the poor performance of the gel-NB/PEG4SH 20 000 formulation as discussed in sections 3.4–3.6 it was not assessed towards biological

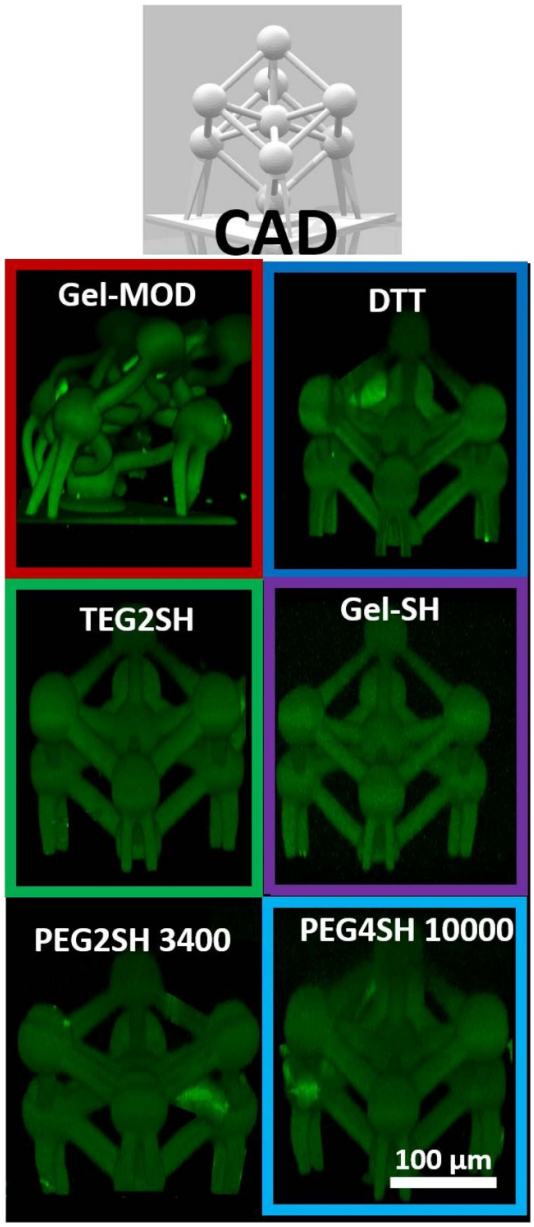

Figure 8. Example of the improved 2PP performance of the different thiol-ene formulations as opposed to the conventional gel-MOD. (all structures written at 100 mm s^{-1} and 100 mW laser power using 0.68 molar of P2CK).

performance. The other formulations were subjected to a cell encapsulation assay by preparing hydrogel formulations consisting of the hydrogel precursors (i.e. gel-MOD or gel-NB and the corresponding thiolated crosslinker, 2 mol% LAP corresponding to around 0.55 mM which is below the cytotoxic limit (i.e. 1.12 mM) [28]) at a total gelatin concentration of 7.5 w/v% and 500 000 GFP-labelled ASCs ml^{-1}. The samples were crosslinked for 10 min using UV-A irradiation and the metabolic activity and cellular morphology of the encapsulated cells was assessed at specific time points using a Presto blue assay and LSM respectively.

When examining the cell morphology over time (figure 9 and zoomed in figures S6–S11), clear differences can be observed between the different formulations. Cells start to remodel the hydrogel matrix sooner in the formulations applying the low molar mass crosslinkers (i.e. DTT and TEG2SH) which is evidenced by an increase in average cell length (figure 10(a)). The fact that this is observed first with the low molar mass crosslinkers is anticipated. First of all, these hydrogels are the softest, which is known to enhance matrix remodeling [19, 65] (figure 3(a)). Because all hydrogels were immediately crosslinked after pipetting; the gel-NB/PEG4SH 10 000 are the stiffest hydrogels (figure 3(d)).

Secondly, remodelling of the matrix occurs via enzymatic cleavage of the gelatin backbone by collagenase between Gly and Ile in Gly-Pro-Gln-Gly-Ile-Ala-Gly-Gln sequences [1, 39]. Because the hydrogels obtained using TEG2SH and DTT only link 2 norbornene functionalities to each other in each junction knot, cleavage of part of the backbone will have a more drastic effect on the network density in comparison to for example gel-MOD or gel-NB/gel-SH hydrogels where every junction knot consists of multiple methacrylamide or thiol/norbornene links similar to the photo-cleavage discussed in section 3.6. Therefore remodeling occurs later (i.e. $\geqslant$7 d; figures 7 and 8(a)) in hydrogel systems with a higher number of thiol functionalities per crosslinker. Consequently, remodeling should occur last in the gel-NB/gel-SH hydrogels with around 14 thiols/crosslinker. However, after 16 d of culture, the cell length is significantly higher in these hydrogels in comparison to the PEG4SH 10 000 hydrogels with 4 thiols/crosslinker due to the fact that the gel-SH crosslinker is also prone to enzymatic degradation, which counterbalances this effect.

The remodeling of the matrix occurs slowest in the gel-MOD hydrogels despite the softer gel in comparison to the gel-NB/PEG4SH 10 000 due to the presence of the kinetic chains which link more functionalities into one junction knot as previously mentioned.

Another aspect to assess biocompatibility is monitoring of the metabolic activity of the cells, which is related to the cellular activity (figure 10(b)) [66]. In this respect, after one day of encapsulation, no significant differences are observed between the different thiol-ene systems and the gel-MOD reference. Although after 2 and 4 d of culture, the gel-MOD reference exhibits a significantly higher metabolic activity in comparison to the PEG containing formulations, while there are no significant differences between the different thiol-ene systems as such. After 8 d of culture, there are no significant differences between the thiol-ene systems and the gel-MOD benchmark any longer. Furthermore, after 14 d, the TEG2SH, PEG4SH 10 000 and gel-SH-containing systems even significantly outperform the gel-MOD.

Therefore, it can be concluded that all assessed thiol-ene systems exhibit at least a comparable

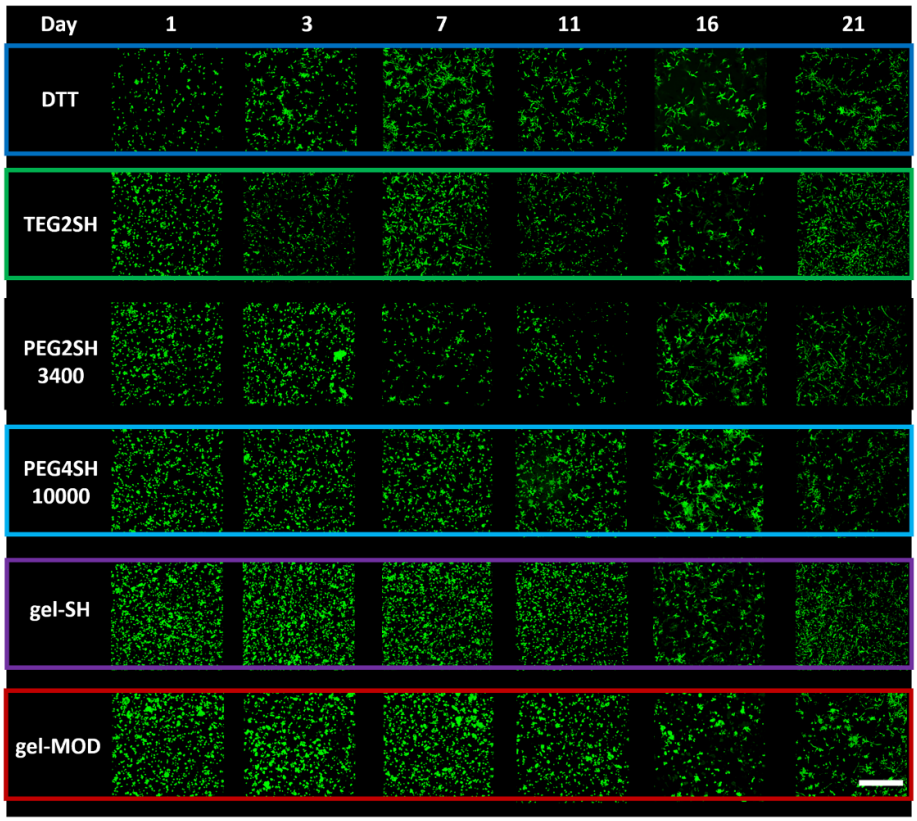

Figure 9. *Z*-stack confocal LSM images of GFP labelled ASCs encapsulated in the different hydrogel formulations after 10 min UV crosslinking at different time points. (scale bar represents 500 μm).

biocompatibility to gel-MOD, irrespective of the applied crosslinker. Additionally, they exhibit more favorable crosslinking kinetics, which can significantly decrease the processing times (section 3.2). In addition, varying the crosslinker provides additional control over the mechanical properties, while maintaining the amount of cell-interactive functionalities (i.e. RGD) [1, 18]. Finally, the mechanical properties can further be fine-tuned by varying the thiol/ene ratio as also previously reported [1, 16, 18].

Another relevant aspect for bioink components, is the toxicity before crosslinking, or the „dark toxicity‘, as depending on the processing duration, the cells will be in the presence of these components for a considerable time. Therefore, the toxicity of the different components was screened at concentrations to yield hydrogels with a gelatin content of 10, 7.5 or 5 w/v%. To this end, a confluent monolayer of GFP-labelled ASCs was exposed to these components for 2 h, followed by component removal and 24 h of incubation. Next, the metabolic activity of the cells was determined (figure 10(c)). Two hours was selected as a relevant time frame, as this is a reasonable estimation of a long printing process, during which the cells would be in contact with the un-crosslinked components. This assay indicated some considerable cytotoxicity of the low molar mass thiolated crosslinkers (i.e. DTT and TEG2SH) at all assessed concentrations (figure 10(c)). This is probably a consequence of the fact that these molecules are small enough to penetrate the cell membrane, as also previously observed for low molar mass PI [55]. Once inside the cell membrane, the thiols present on these crosslinkers can interact with thiols present within the cytoplasm such as kinases, transcription factors, and phosphatases, thereby reducing-, or forming disulphide bonds [67–69]. Consequently, this dark toxicity was not observed for the high molar mass crosslinkers (i.e. PEG2SH 3400, PEG4SH 10 000 and gel-SH). In terms of gelatin materials, a comparable biocompatibility is observed between gel-NB and gel-MOD at 7.5 w/v%, whereas at high concentrations, gel-NB even appears to be less cytotoxic. Therefore, gel-NB thiol-ene systems prove to be suitable alternatives for the very popular gel-MOD in terms of biocompatibility when selecting the correct crosslinker.

3.7.2. Primary cell culture

Since immortalized cell lines are typically very robust, the obtained results were verified by encapsulation of primary ASCs. To this end, the most representative hydrogel formulations where assessed in combination with primary hASCs. To this end, hASCs were encapsulated as mentioned earlier and the cell viability was analysed through a Ca-AM and propidium iodide (PI) staining at day 1, 3 and 7 (figure 11).

The hydrogels resulted in a cell viability >70% for all tested formulations, meaning that all compositions

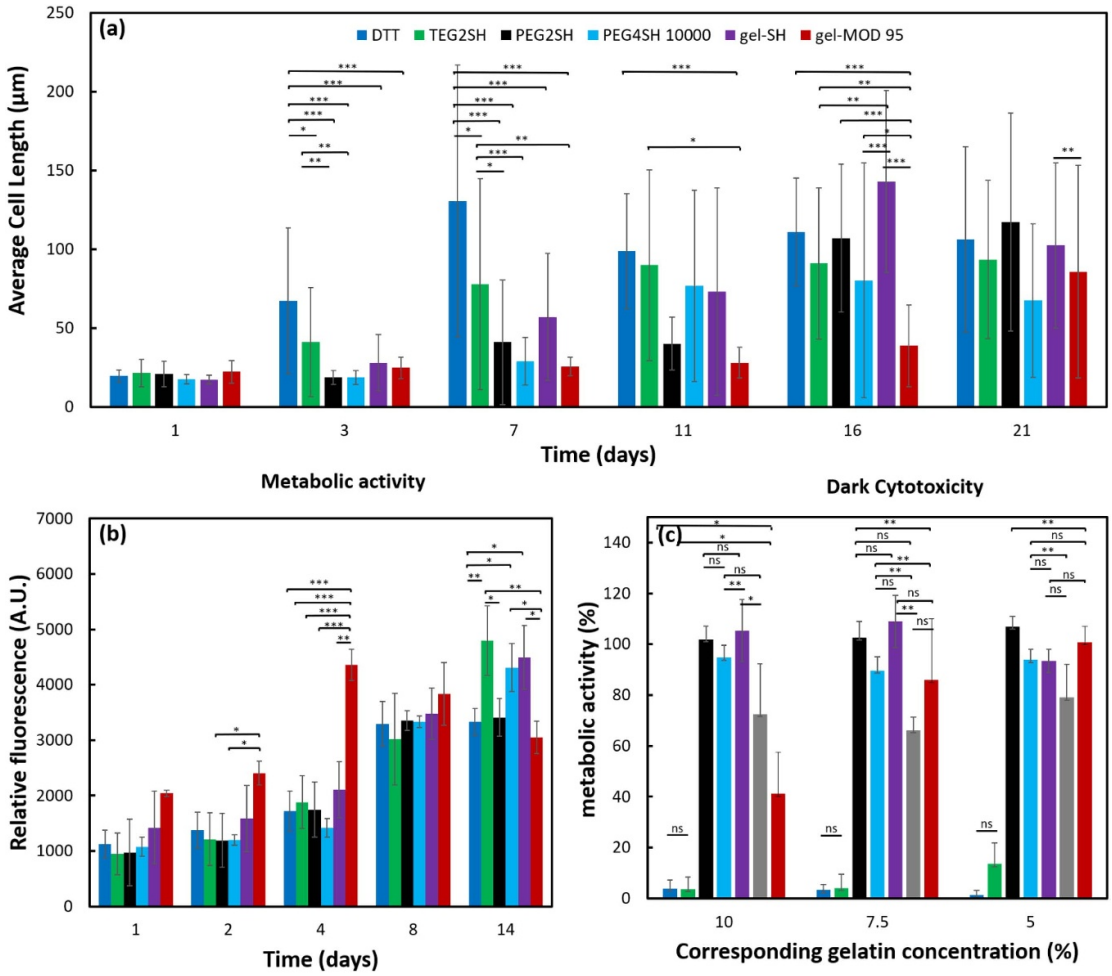

Figure 10. Average lengths of cells embedded in the different hydrogel formulations at different time points (a) Associated metabolic activity at different time points (b). Dark cytotoxicity of the different components of the hydrogel formulations for three different corresponding gelatin concentrations (c). All statistically significant differences are denoted with $*p < 0.05$, $**p < 0.01$, $***p < 0.005$, except for panel (c) in which all differences are significant with $p < 0.005$ unless denoted otherwise with ns representing no statistical difference.

can be considered biocompatible (figure 12). However, a significantly lower cell viability was observed for the formulation containing DTT as compared to the other formulations, for all time points. The aforementioned 'dark' toxicity of DTT can explain the lower cell viability observed. Wu *et al* have already observed an increase in cytotoxicity corresponding to an increase in DTT concentration [70]. Nevertheless, no significant differences were observed based on the metabolic activity of the GFP-labelled ASCs encapsulated in the DTT composition compared to the other thiolated crosslinkers (figure 10). There are several reasons which could explain the difference between the cell viability and metabolic activity. First, for the metabolic activity, immortalized GFP-labelled ASCs were used, which might be more resistant to the cytotoxic effects of DTT. However, a more likely explanation for the discrepancy is the fact that cells which undergo stress will exhibit an increase in metabolic activity [71]. This is supported by the less densely populated construct observed for the GFP-labelled cells when DTT is used (figures 9 and S6).

4. Conclusions

Thiol-norbornene gelatin hydrogels prove to be very relevant alternatives for the widely used gel-MOD as bioink or biomaterial ink (component) for biofabrication purposes. The use of thiol-ene photo-click chemistry allows to further tune the hydrogel properties in terms of reactivity, processability, mechanical properties and biological response by varying the thiolated crosslinker. Crosslinkers with a higher number of thiols (i.e. gel-SH or PEG4SH 10 000) result in stiffer gels, thereby better mimicking the mechanical properties of the widely used gel-MOD in combination with more favorable crosslinking kinetics. The selection of the most appropriate crosslinker also depends on the processing method of the gelatin hydrogel. When direct crosslinking from solution is desired, superior mechanical properties are obtained with PEG4SH 10 000. When comparable mechanical properties and a low water uptake capacity are desired, gel-SH-type crosslinkers are preferred. If crosslinking is desired from a physical

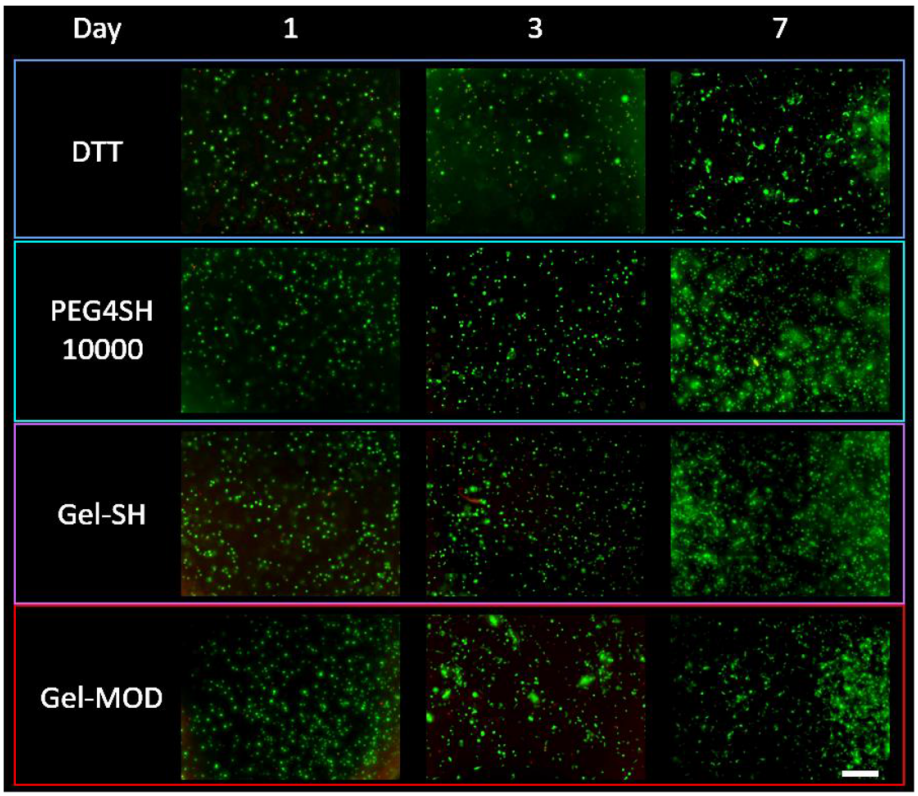

Figure 11. Z-stack of the live/dead staining using Ca-AM and PI on encapsulated primary ASCs in the different hydrogel formulations at day 1, 3 and 7. The scale bar represents 500 μm.

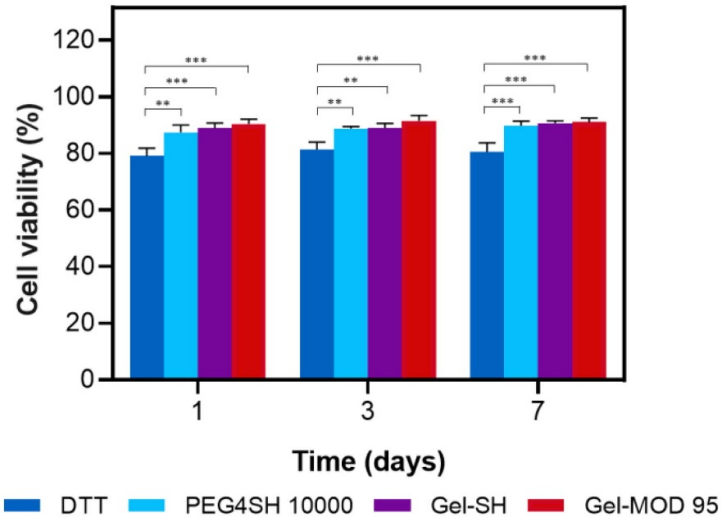

Figure 12. The cell viability of encapsulated ASCs based on Ca-AM and PI staining. All statistically significant differences are depicted with $^{*}p < 0.05$, $^{**}p < 0.01$, $^{***}p < 0.005$.

gel, the low molar mass or gel-SH crosslinkers are preferred because phase separation can occur with the high molar mass PEG crosslinkers resulting in a heterogeneous network. In this respect, superior mechanical properties are obtained for the conventional gel-MOD, followed closely by the gel-NB/gel-SH system that also benefits from the physical gelation prior to crosslinking. Additionally, the gel-NB/gel-SH system provides the best mimic for gel-MOD in terms of physicochemical properties with the added benefit that it is fully biodegradable without the presence of residual non-degradable polymer chains.

In terms of biological performance, no significant differences in metabolic activity were observed between the different gel-NB formulations and the gel-MOD benchmark, indicating a comparable, favorable cytocompatibility. However, the type of

crosslinker does influence the cellular induced matrix remodeling of encapsulated cells. The low molar mass crosslinkers (i.e. TEG2SH and DTT) induce faster matrix remodeling in comparison to formulations with high molar mass crosslinkers and gel-MOD. In this respect, not only the mechanical properties of the hydrogel are of importance but also the type of crosslinks present in the hydrogel. The stiffest formulation containing PEG4SH 10 000, still exhibits matrix remodeling prior to gel-MOD because of the different network architecture (i.e. no kinetic chains). Furthermore, the 'dark toxicity' of the components was also assessed to assess suitability for longer printing times, indicating considerable toxicity for the low molar mass crosslinkers (i.e. TEG2SH and DTT). This effect also resulted in a decreased cell viability upon primary cell encapsulation. It is anticipated that this originates from cell membrane penetration and subsequent interaction with native thiols as high molar mass crosslinkers did not exhibit significant cytotoxicity. Furthermore, gel-NB and gel-MOD exhibited a comparable dark cytotoxicity.

The real benefit of the thiol-ene systems lies in for the use of light-based AM, where the photo-reactivity has a great influence on the attainable writing speeds and associated processing times. This is especially relevant for high-resolution laser scanning-based systems such as SLA or 2PP or DLP based systems. It was shown that substantially (i.e. 20-fold) lower laser powers could be applied to crosslink the thiol-ene formulations, regardless of the applied crosslinker. However, the applied crosslinker does have a large influence on the volumetric swelling ratio and associated differences in CAD-CAM fidelity. The high molar mass, bifunctional PEG crosslinker (PEG2SH 3400) exhibited the highest swelling ratio over the entire processing range due to the low amount of thiol functionalities, the large distance between two crosslinks and the highly hydrophilicity of the crosslinker. The least swelling was obtained for the crosslinker with the highest number of thiols (i.e. gel-SH).

However, at high average laser powers, a specific non-anticipated increase in swelling was observed in all formulations due to photo-cleavage of amide bonds in the gelatin backbone. This effect was most pronounced for the low molar mass bifunctional thiolated crosslinkers (i.e. DTT and TEG2SH) while being absent for the highly functional gel-SH crosslinker as well as for gel-MOD. In the low molar mass crosslinker systems, fewer bonds need to be cleaved to result in real channels in the hydrogel.

In conclusion, the most promising thiol-ene alternative for gel-MOD is the gel-NB/gel-SH formulation, as it mimics the mechanical properties of gel-MOD, is also benefitted by the physical gelation behaviour prior to crosslinking, exhibits comparable cytotoxicity, contains only fully biodegradable and biointeractive components, and exhibits the best shape fidelity thereby being the least susceptible to photocleavage.

Acknowledgments

Jasper Van Hoorick, Lana Van Damme and Liesbeth Tytgat were granted an FWO-SB PhD grant provided by the Research Foundation Flanders (FWO, Belgium). The FWO-FWF grant (a bilateral Research foundation Flanders—Austrian Science fund project #I2444N28) is acknowledged for financial support. S Van Vlierberghe thanks the FWO for financial support under the form of research grants (Grant Nos. G005616N, G0F0516N, FWOKN273, G044516N) as well as Ghent University for funding a starting grant through the Special Research Fund.

ORCID iDs

Jasper Van Hoorick https://orcid.org/0000-0002-1468-3936
Lana Van Damme https://orcid.org/0000-0003-0102-1850
Hugo Thienpont https://orcid.org/0000-0003-0483-0960
Aleksandr Ovsianikov https://orcid.org/0000-0001-5846-0198
Sandra Van Vlierberghe https://orcid.org/0000-0001-7688-1682

References

[1] Van Hoorick J, Tytgat L, Dobos A, Ottevaere H, Van Erps J, Thienpont H, Ovsianikov A, Dubruel P and Van Vlierberghe S 2019 (Photo-)crosslinkable gelatin derivatives for biofabrication applications *Acta Biomater.* **97** 46–73
[2] Li Z, Qu T, Ding C, Ma C, Sun H, Li S and Liu X 2015 Injectable gelatin derivative hydrogels with sustained vascular endothelial growth factor release for induced angiogenesis *Acta Biomater.* **13** 88–100
[3] Pan J F, Yuan H F, Guo C A, Liu J, Geng X H, Fei T, Li S, Fan W S, Mo X M and Yan Z Q 2015 One-step cross-linked injectable hydrogels with tunable properties for space-filling scaffolds in tissue engineering *RSC Adv.* **5** 40820–30
[4] Van Nieuwenhove I, Salamon A, Peters K, Graulus G, Martins J C, Frankel D, Kersemans K, De Vos F, Van Vlierberghe S and Dubruel P 2016 Gelatin- and starch-based hydrogels. part A: hydrogel development, characterization and coating *Carbohydr. Polym.* **152** 129–39
[5] Graulus G-J, Mignon A, Van Vlierberghe S, Declercq H, Fehér K, Cornelissen M, Martins J C and Dubruel P 2015 Cross-linkable alginate-graft-gelatin copolymers for tissue engineering applications *Eur. Polym. J.* **72** 494–506
[6] Steyaert I, Rahier H, Van Vlierberghe S, Olijve J and De Clerck K 2016 Gelatin nanofibers: analysis of triple helix dissociation temperature and cold-water-solubility *Food Hydrocoll.* **57** 200–8
[7] Anon 1979 Gelatin, Rep. No. 58, 9000-70-8 FDA's SCOGS
[8] Schrieber R and Gareis H 2007 *Gelatine Handbook: Theory and Industrial Practice* (Weinheim: Wiley-VCH)
[9] Rose J B, Pacelli S, El Haj A J, Dua H S, Hopkinson A, White L J and Rose F R A J 2014 Gelatin-based materials in ocular tissue engineering *Materials* **7** 3106–35
[10] Schacht E, Van Den Bulcke A I, Delaey B and Draye J-P 2002 New medicaments based on polymers composed of

methacrylamide-modified gelatin, *EUR Patent Specification* WO/1998/055161
[11] Van Den Bulcke A I, Bogdanov B, De Rooze N, Schacht E H, Cornelissen M and Berghmans H 2000 Structural and rheological properties of methacrylamide modified gelatin hydrogels *Biomacromolecules* **1** 31–38
[12] Klotz B J, Gawlitta D, Rosenberg A J W P, Malda J and Melchels F P W 2016 Gelatin-methacryloyl hydrogels: towards biofabrication-based tissue repair *Trends Biotechnol.* **34** 394–407
[13] Van Hoorick J, Delaey J, Van Erps J, Thienpont H, Dubruel P, Zakaria N, Koppen C, Van Vlierberghe S and Van Den Bogerd B 2020 Designer Descemet membranes containing PDLLA and functionalized gelatins as corneal endothelial scaffold *Adv. Healthc. Mater.* **9** 2000760
[14] Bertlein S, Brown G, Lim K S, Jungst T, Boeck T, Blunk T, Tessmar J, Hooper G J, Woodfield T B F and Groll J 2017 Thiol-ene clickable gelatin: a platform bioink for multiple 3D biofabrication technologies *Adv. Mater.* **29** 1703404
[15] Heffernan J M, Overstreet D J, Le L D, Vernon B L and Sirianni R W 2015 Bioengineered scaffolds for 3D analysis of glioblastoma proliferation and invasion *Ann. Biomed. Eng.* **43** 1965–77
[16] Van Hoorick J *et al* 2018 Highly reactive thiol-norbornene photo-click hydrogels: toward improved processability *Macromol. Rapid Commun.* **39** 1800181
[17] Levato R, Jungst T, Scheuring R G, Blunk T, Groll J and Malda J 2020 From shape to function: the next step in bioprinting *Adv. Mater.* **32** 1906423
[18] Mũnoz Z, Shih H and Lin -C-C 2014 Gelatin hydrogels formed by orthogonal thiol–norbornene photochemistry for cell encapsulation *Biomater. Sci.* **2** 1063
[19] Dobos A *et al* 2019 Thiol–gelatin–norbornene bioink for laser-based high-definition bioprinting *Adv. Healthc. Mater.* **9** 1900752
[20] Cramer N B and Bowman C N 2017 Thiol-ene chemistry *Chemoselective and Bioorthogonal Ligation Reactions: Concepts and Applications, Volume 1* ed W R Algar, P E Dawson and I L Medintz (Weinheim: Wiley-VCH) vol **2011** 117–45
[21] Hoyle C E, Lee T Y and Roper T 2004 Thiol-enes: chemistry of the past with promise for the future *J. Polym. Sci.* A **42** 5301–38
[22] Dobos A, Gantner F, Markovic M, Van Hoorick J, Tytgat L, Van Vlierberghe S and Ovsianikov A 2020 On-chip high-definition bioprinting of microvascular structures *Biofabrication* (https://doi.org/10.1088/1758-5090/abb063)
[23] Tytgat L, Van Damme L, Van Hoorick J, Declercq H, Thienpont H, Ottevaere H, Blondeel P, Dubruel P and Van Vlierberghe S 2019 Additive manufacturing of photo-crosslinked gelatin scaffolds for adipose tissue engineering *Acta Biomater.* **94** 340–50
[24] Tytgat L, Dobos A, Markovic M, Van Hoorick J, Bray F, Thienpont H, Ottevaere H, Dubruel P, Ovsianikov A and Van Vlierberghe S 2020 High-resolution 3D bioprinting of photo-crosslinkable recombinant collagen to serve tissue engineering applications *Biomacromolecules* **21** 3997–4007
[25] Van Vlierberghe S, Fritzinger B, Martins J C and Dubruel P 2010 Hydrogel network formation revised: high-resolution magic angle spinning nuclear magnetic resonance as a powerful tool for measuring absolute hydrogel cross-link efficiencies *Appl. Spectrosc.* **64** 1176–80
[26] Kanao M, Otake A, Tsuchiya K and Ogino K 2012 Stereo-selective synthesis of 5-norbornene-2-*exo*-carboxylic acid—rapid isomerization and kinetically selective hydrolysis *Int. J. Org. Chem.* **02** 26–30
[27] Van Vlierberghe S, Schacht E and Dubruel P 2011 Reversible gelatin-based hydrogels: finetuning of material properties *Eur. Polym. J.* **47** 1039–47
[28] Markovic M, Van Hoorick J, Hölzl K, Tromayer M, Gruber P, Nürnberger S, Dubruel P, Van Vlierberghe S, Liska R and Ovsianikov A 2015 Hybrid tissue engineering scaffolds by combination of three-dimensional printing and cell photoencapsulation *J. Nanotechnol. Eng. Med.* **6** 021001
[29] Van Hoorick J, Gruber P, Markovic M, Tromayer M, Van Erps J, Thienpont H, Liska R, Ovsianikov A, Dubruel P and Van Vlierberghe S 2017 Cross-linkable gelatins with superior mechanical properties through carboxylic acid modification: increasing the two-photon polymerization potential *Biomacromolecules* **18** 3260–72
[30] Knezevic L, Schaupper M, Mühleder S, Schimek K, Hasenberg T, Marx U, Priglinger E, Redl H and Holnthoner W 2017 Engineering blood and lymphatic microvascular networks in fibrin matrices *Front. Bioeng. Biotechnol.* **5** 25
[31] Lunzer M, Shi L, Andriotis O G, Gruber P, Markovic M, Thurner P J, Ossipov D, Liska R and Ovsianikov A 2018 A modular approach to sensitized two-photon patterning of photodegradable hydrogels *Angew. Chem. Int. Ed.* **57** 15122–7
[32] Lim K S *et al* 2018 Bio-resin for high resolution lithography-based biofabrication of complex cell-laden constructs *Biofabrication* **10** 034101
[33] Sirova M, Van Vlierberghe S, Matyasova V, Rossmann P, Schacht E, Dubruel P and Rihova B 2014 Immunocompatibility evaluation of hydrogel-coated polyimide implants for applications in regenerative medicine *J. Biomed. Mater. Res.* A **102** 1982–90
[34] Pfitzner K E and Moffatt J G 1963 A new and selective oxidation of alcohols *J. Am. Chem. Soc.* **85** 3027–8
[35] Nair D P, Podgórski M, Chatani S, Gong T, Xi W, Fenoli C R and Bowman C N 2013 The thiol-Michael addition click reaction: a powerful and widely used tool in materials chemistry *Chem. Mater.* **26** 724–44
[36] Gramlich W M, Kim I L and Burdick J A 2013 Synthesis and orthogonal photopatterning of hyaluronic acid hydrogels with thiol-norbornene chemistry-supporting information *Biomaterials* **34** 9803–11
[37] Lin -C-C, Ki C S and Shih H 2015 Thiol-norbornene photo-click hydrogels for tissue engineering applications *J. Appl. Polym. Sci.* **132** 1–11
[38] Dobos A, Steiger W, Theiner D, Gruber P, Lunzer M, Van Hoorick J, Van Vlierberghe S and Ovsianikov A 2019 Screening of two-photon activated photodynamic therapy sensitizers using a 3D osteosarcoma model *Analyst* **144** 3056–63
[39] Greene T, Lin T, Andrisani O M and Lin C 2017 Comparative study of visible light polymerized gelatin hydrogels for 3D culture of hepatic progenitor cells *J. Appl. Polym. Sci.* **44585** 1–10
[40] Greene T and Lin C 2015 Modular cross-linking of gelatin-based thiol−norbornene hydrogels for in vitro 3D culture of hepatocellular carcinoma cells *ACS Biomater. Sci. Eng.* **1** 1314–23
[41] Li L, Lu C, Wang L, Chen M, White J, Hao X, McLean K M, Chen H and Hughes T C 2018 Gelatin-based photocurable hydrogels for corneal wound repair *ACS Appl. Mater. Interfaces* **10** 13283–92
[42] Russo L, Sgambato A, Visone R, Occhetta P, Moretti M, Rasponi M, Nicotra F and Cipolla L 2016 Gelatin hydrogels via thiol-ene chemistry *Monatsh. Chem.* **147** 587–92
[43] Billiet T, Van Gasse B, Gevaert E, Cornelissen M, Martins J C and Dubruel P 2013 Quantitative contrasts in the photopolymerization of acrylamide and methacrylamide-functionalized gelatin hydrogel building blocks *Macromol. Biosci.* **13** 1531–45
[44] Mccall J D and Anseth K S 2012 Thiol−ene photopolymerizations provide a facile method to encapsulate proteins and maintain their bioactivity *Biomacromolecules* **13** 2410–7
[45] Fairbanks B D, Schwartz M P, Bowman C N and Anseth K S 2009 Photoinitiated polymerization of PEG-diacrylate with lithium phenyl-2,4,6-trimethylbenzoylphosphinate: polymerization rate and cytocompatibility *Biomaterials* **30** 6702–7

[46] Lim K S, Schon B S, Mekhileri N V, Brown G C J, Chia C M, Prabakar S, Hooper G J and Woodfield T B F 2016 New visible-light photoinitiating system for improved print fidelity in gelatin-based bioinks *ACS Biomater. Sci. Eng.* **2** 1752–62
[47] Shih H and Lin -C-C 2014 Crosslinking and degradation of step-growth hydrogels formed by thiol-ene photo-click chemistry *Biomacromolecules* **13** 2003–12
[48] Stevens R, Stevens L and Price N C 1983 The stabilities of various thiol compounds used in protein purifications *Biochem. Educ.* **11** 70
[49] Eckert T and Abetz V 2020 Polymethacrylamide—an underrated and easily accessible upper critical solution temperature polymer: green synthesis via photoiniferter reversible addition–fragmentation chain transfer polymerization and analysis of solution behavior in water/ethanol mixtures *J. Polym. Sci.* **58** 3050–60
[50] Hölzl K, Lin S, Tytgat L, Van Vlierberghe S, Gu L and Ovsianikov A 2016 Bioink properties before, during and after 3D bioprinting *Biofabrication* **8** 032002
[51] Billiet T, Gevaert E, De Schryver T, Cornelissen M and Dubruel P 2014 The 3D printing of gelatin methacrylamide cell-laden tissue-engineered constructs with high cell viability *Biomaterials* **35** 49–62
[52] Pereira R F and Bartolo P J 2015 3D bioprinting of photocrosslinkable hydrogel constructs *J. Appl. Polym. Sci.* **132** 42458
[53] Melchels F P W, Dhert W J A, Hutmacher D W and Malda J 2014 Development and characterisation of a new bioink for additive tissue manufacturing *J. Mater. Chem.* B **2** 2282
[54] Ma S, Natoli M, Liu X, Neubauer M P, Watt F M, Fery A and Huck W T S 2013 Monodisperse collagen–gelatin beads as potential platforms for 3D cell culturing *J. Mater. Chem.* B **1** 5128
[55] Tromayer M, Gruber P, Markovic M, Rosspeintner A, Vauthey E, Redl H, Ovsianikov A and Liska R 2017 A biocompatible macromolecular two-photon initiator based on hyaluronan *Polym. Chem.* **8** 451–60
[56] Tromayer M, Dobos A, Gruber P, Ajami A, Dedic R, Ovsianikov A and Liska R 2018 A biocompatible diazosulfonate initiator for direct encapsulation of human stem cells *via* two-photon polymerization *Polym. Chem.* **9** 3108–17
[57] Heo Y J, Iwanaga S and Takeuchi S 2012 A nanochannel fabrication technique by two-photon direct laser writing *Proc. IEEE Int. Conf. Micro Electro Mech. Syst.* pp 997–1000
[58] Kumar R and Anantha Ramakrishna S 2017 Microstructuring by two-photon polymerization using a sub-nanosecond laser *Curr. Sci.* **112** 1668
[59] Zipfel W R, Williams R M and Webb W W 2003 Nonlinear magic: multiphoton microscopy in the biosciences *Nat. Biotechnol.* **21** 1369–77
[60] Marek B and Lerch E 1965 Photodegradation and yellowing of polyamides *J. Soc. Dyers Colour.* **81** 481–7
[61] Shamey R and Sinha K 2003 A review of degradation of nylon 6.6 as a results of exposure to environmental conditions *Rev. Prog. Color. Relat. Top.* **33** 93–107
[62] Do C H, Pearce E M, Bulkin B J and Reimschuessel H K 1987 FT–IR spectroscopic study on the photo- and photooxidative degradation of nylons *J. Polym. Sci.* A **25** 2301–21
[63] Melchels F P W, Feijen J and Grijpma D W 2010 A review on stereolithography and its applications in biomedical engineering *Biomaterials* **31** 6121–30
[64] Groll J, Burdick J A, Cho D, Derby B, Gelinsky M, Heilshorn S C, Jüngst T and Malda J 2018 A definition of bioinks and their distinction from biomaterial inks *Biofabrication* **11** 013001
[65] Žigon-Branc S, Markovic M, Van Hoorick J, Van Vlierberghe S, Dubruel P, Zerobin E, Baudis S and Ovsianikov A 2019 Impact of hydrogel stiffness on differentiation of human adipose-derived stem cell microspheroids *Tissue Eng.* A **25** 1369–80
[66] Wang X, Qin X-H, Hu C, Terzopoulou A, Chen X-Z, Huang T-Y, Maniura-Weber K, Pané S and Nelson B J 2018 3D printed enzymatically biodegradable soft helical microswimmers *Adv. Funct. Mater.* **1804107** 1804107
[67] Koshy S T, Desai R M, Joly P, Li J, Bagrodia R K, Lewin S A, Joshi N S and Mooney D J 2016 Click-crosslinked injectable gelatin hydrogels *Adv. Healthc. Mater.* **5** 541–7
[68] Mannervik B, Axelsson K, Sundewall A C and Holmgren A 1983 Relative contributions of thioltransferase-and thioredoxin-dependent systems in reduction of low-molecular-mass and protein disulphides *Biochem. J.* **213** 519–23
[69] López-Mirabal H R and Winther J R 2008 Redox characteristics of the eukaryotic cytosol *Biochim. Biophys. Acta Mol. Cell. Res.* **1783** 629–40
[70] Wu F, Ju X J, He X H, Jiang M Y, Wang W, Liu Z, Xie R, He B and Chu L Y 2016 A novel synthetic microfiber with controllable size for cell encapsulation and culture *J. Mater. Chem.* B **4** 2455–65
[71] Rai Y, Pathak R, Kumari N, Sah D K, Pandey S, Kalra N, Soni R, Dwarakanath B S and Bhatt A N 2018 Mitochondrial biogenesis and metabolic hyperactivation limits the application of MTT assay in the estimation of radiation induced growth inhibition *Sci. Rep.* **8** 1–15